

<https://doi.org/10.1038/s43247-024-01666-3>

Microbial cycling contributes to the release of dissolved inorganic phosphate into the groundwater of floodplain aquifers



Yao Li^{1,2,3}, Harald Neidhardt², Huaming Guo^{1,3} , Christiane Nagel², Wen Shao², Chen Yu¹, Bo Zhao¹, Dou Chen¹, Wei Xiu¹ & Yvonne Oelmann² 

Little is known about biological processes controlling inorganic phosphate (PO_4) in groundwater ecosystems. Here we present analyses of groundwater samples from the Hetao Basin, China that show an increasing contribution of microbial cycling to groundwater PO_4 from oxic to anoxic conditions along a flow path with phosphate-bound oxygen isotopes ($\delta^{18}\text{O}_{\text{PO}_4}$). Under oxic conditions, although 25–47% of the dissolved PO_4 inherited the initial source signal of igneous apatite, groundwater $\delta^{18}\text{O}_{\text{PO}_4}$ reflected a pronounced impact of intracellular enzymatic cycling. Under anoxic conditions, dissolved PO_4 carried a nearly exclusive equilibrium isotope signal, which was probably due to (i) release of PO_4 with an equilibrium $\delta^{18}\text{O}_{\text{PO}_4}$ from Fe(III) oxides, as a result of Fe(III) reduction in the presence of Fe(III)- and sulfate-reducing bacteria; and/or (ii) cumulative microbial cycling of dissolved PO_4 with increasing groundwater residence time. Our study highlights that PO_4 in groundwater is tightly microbially cycled under a wide range of redox conditions and microbial cycling contributes to the release of PO_4 in groundwater.

In recent years, the potential environmental impact of high concentrations of inorganic phosphate (PO_4) in groundwater ecosystems has received increasing attention^{1–3}. For instance, groundwater with high PO_4 concentrations can be transported to surface waters and induce eutrophication^{4,5}. Moreover, high concentrations of dissolved PO_4 in groundwater can promote the mobility of toxic arsenic via competitive adsorption^{6,7}, which poses a threat to groundwater quality and human health, especially in SE Asia⁸. Therefore, it is important to reveal the biogeochemical processes that are involved in the release of dissolved PO_4 in groundwater.

Previous studies focused on the anthropogenic inputs of PO_4 into groundwater at contaminated sites (i.e., farmlands^{9–11} and wastewater treatment plants^{12–14}), but recent studies highlighted the importance of geogenic, aquifer-internal PO_4 release in groundwater of floodplain aquifers worldwide^{15–17}. Generally, organic matter (OM) degradation, reductive dissolution of Fe(III) oxides and apatite dissolution are regarded as the three main processes that release PO_4 into the groundwater^{18–20}. In aquatic ecosystems, other biological processes may also contribute to PO_4 release.

Under natural conditions, enzymatically mediated reactions release PO_4 from organic phosphorus compounds (P_{org}) to meet the demand of microbial growth²¹. The regenerated PO_4 eventually undergoes microbial uptake and intracellular cycling, and is finally released back to the extracellular environment²¹. Previous studies demonstrated that microbial cycling is an important process that releases PO_4 in soil, lakes, and marine environments^{22–26}. In floodplain aquifers, it is known that microbial activity is linked to OM degradation and Fe(III) reduction²⁷. However, whether released PO_4 has been utilized by microorganisms and how it contributes to the increase of dissolved PO_4 in floodplain aquifers remains unclear.

In soils and marine environments, it is known that microbial activity and PO_4 utilization are affected by changing redox conditions^{28–30}. On the one hand, redox conditions directly constrain the rate of microbial respiration and activity, therefore the ability of microbes to utilize PO_4 ^{29,31}. On the other hand, microbial PO_4 utilization is indirectly influenced by redox conditions^{30,32}. Under anoxic conditions, the reductive dissolution of Fe(III) oxides can release surface-adsorbed, occluded and/or co-precipitated PO_4 ^{33,34}, thus potentially enhancing the PO_4 bioavailability and microbial

¹State Key Laboratory of Biogeology and Environmental Geology, School of Water Resources and Environment, China University of Geosciences, 100083 Beijing, China. ²Geoecology, University of Tübingen, 72070 Tübingen, Germany. ³MOE Key Laboratory of Groundwater Circulation and Environment Evolution, China University of Geosciences, 100083 Beijing, China.  e-mail: hmguo@cugb.edu.cn; yvonne.oelmann@uni-tuebingen.de

PO₄ utilization. Previous studies in floodplains have demonstrated tight constraints of redox conditions on microbial activity^{35,36} and PO₄ release in aquifers³⁷. Furthermore, Fe(III) oxides are abundant in aquifer sediments serving as an important sink for PO₄, which might eventually be released under anoxic conditions. Therefore, the contribution of microbially cycled PO₄ could either be decreased or increased under anoxic as compared to oxic conditions in floodplain aquifers.

In the past decade, the stable isotope ratio of PO₄-O ($\delta^{18}\text{O}_{\text{PO}_4}$) has emerged as a useful tool for identifying PO₄ sources^{38–41} and the involvement of microbial activity in PO₄ cycling in surface aquatic ecosystems^{42–44}. Under typical groundwater temperature, pressure, and pH conditions, the P–O bonds in PO₄ are resistant to inorganic hydrolysis^{45,46}. However, enzymatic cleavage of PO₄ is associated with an exchange of O atoms from ambient water accompanied by isotopic fractionation^{47–49}. In particular, the intracellular enzyme pyrophosphatase imposes a temperature-dependent equilibrium isotopic fractionation of O between PO₄ and ambient water^{50,51}. As a result, $\delta^{18}\text{O}_{\text{PO}_4}$ values may shift from the original source signature (i.e., minerals in the bedrock from which the PO₄ was originally released) towards isotopic equilibrium values ($\delta^{18}\text{O}_{\text{PO}_4 \text{ equ}}$)^{42,52,53}. Theoretical $\delta^{18}\text{O}_{\text{PO}_4 \text{ equ}}$ values are calculated for a given sample based on the local temperature and $\delta^{18}\text{O}$ of ambient (ground)water ($\delta^{18}\text{O}_{\text{H}_2\text{O}}$)⁵⁰. So far, only a few studies have investigated the $\delta^{18}\text{O}_{\text{PO}_4}$ characteristics of groundwater⁵⁴ and their results showed that $\delta^{18}\text{O}_{\text{PO}_4}$ values may differ from the equilibrium value, possibly reflecting anthropogenic PO₄ inputs^{15,55}. However, in floodplain aquifers, high concentrations of PO₄ and other typical geogenic contaminants are most likely accumulated from long term water–rock interactions^{20,56,57}. Therefore, $\delta^{18}\text{O}_{\text{PO}_4}$ characteristics in groundwater of floodplain aquifers may behave differently, reflecting aquifer-internal PO₄ release processes.

The Hetao Basin is located in the Inner Mongolia Autonomous Region, PR China, where more than 70% of the groundwater has phosphorus (P) concentrations exceeding 50 $\mu\text{g L}^{-1}$, and dissolved P in groundwater predominantly presents in the form of PO₄³⁷. In the aquifer sediments, Fe(III) oxides represent an important source of PO₄ with average contents of adsorbed PO₄-P of 9.1 mg kg^{-1} . The reductive dissolution of Fe(III) oxides is considered as a dominant process releasing PO₄ under anoxic conditions³⁷. Along the groundwater flow path, redox conditions gradually change from oxic to strongly reducing which is associated with a sequence of microbially mediated redox reactions, such as microbial iron oxidation, microbial Fe(III) reduction and microbial sulfate reduction^{58–60} (Fig. 1). There are multiple clay layers in the sediments, separating a shallow (5–40 m bls) and a deep aquifer (40–100 m bls)⁶¹. Our previous investigation showed that dissolved PO₄ concentrations were significantly higher in the deep aquifer than in the shallow aquifer, suggesting a dominant role of in situ geochemical processes in the release of PO₄³⁷. Moreover, we found that

concentrations of NH₄⁺, NO₃[−], and SO₄^{2−}, being potential proxies for anthropogenic inputs^{10,12}, were all significantly lower in the shallow aquifer than in the deep aquifer³⁷. Hence, in this study, we consider a separation of the aquifers from the surface and apply the $\delta^{18}\text{O}_{\text{PO}_4}$ analysis to (1) uncover microbial cycling of PO₄ in groundwater systems and (2) reveal the influence of redox conditions on microbial PO₄ cycling in groundwater of floodplain aquifers.

We found that the contribution of microbial PO₄ cycling to the dissolved PO₄ significantly increased along a groundwater flow path from oxic to anoxic conditions. In the alluvial fan under oxic conditions, although 25–47% of the dissolved PO₄ inherited the initial source signal of igneous apatite, groundwater $\delta^{18}\text{O}_{\text{PO}_4}$ reflected a pronounced impact of intracellular enzymatic cycling by microorganisms. In the flat plain under anoxic conditions, dissolved PO₄ carried a nearly exclusive equilibrium isotope signal. This was probably due to the release of PO₄ with an equilibrium $\delta^{18}\text{O}_{\text{PO}_4}$ value from Fe(III) oxides, as a result of Fe(III) reduction in the presence of Fe(III)- and sulfate-reducing bacteria. Another potentially important aspect was the increasing residence times of groundwater from the alluvial fan (< 125 years) to the flat plain (ca. 600 years), which allowed the dissolved PO₄ to be more microbially cycled and consequently the groundwater $\delta^{18}\text{O}_{\text{PO}_4}$ values gradually approached isotopic equilibrium. We therefore conclude that PO₄ in groundwater is tightly microbially cycled under a wide range of redox conditions, and highlight microbial PO₄ cycling involved in the reductive dissolution of Fe(III) oxides as an overlooked biological process contributing to the release of PO₄ into groundwater.

Results and discussion

The presence of microbial PO₄ cycling in groundwater

Along the groundwater flow path, the $\delta^{18}\text{O}_{\text{H}_2\text{O}}$ of groundwater increased from the alluvial fan (median of −10.6‰) over the transition area (median of −9.9‰) towards the flat plain (median of −8.7‰) (Figs. 2a, 3a). In the basin, groundwater levels gradually decreased from the alluvial fan (about 10 m bls) to the flat plain (about 2 m bls)⁵⁶. The gradually increased $\delta^{18}\text{O}_{\text{H}_2\text{O}}$ values most likely reflected increasing evaporation along the flow path. This was further supported by the increasing TDS values and Cl[−] concentrations (see Supplementary Table S1), agreeing with previous studies^{58,62}. Similar to $\delta^{18}\text{O}_{\text{H}_2\text{O}}$, $\delta^{18}\text{O}_{\text{PO}_4}$ values in groundwater significantly increased ($p < 0.01$) from the alluvial fan (median of +11.7‰) over the transition area (median of +13.4‰) towards the flat plain (median of +15.2‰) (Figs. 2b, 3b). Since abiotic processes have negligible effects on the $\delta^{18}\text{O}_{\text{PO}_4}$ in aquatic ecosystems^{63,64}, the increase in $\delta^{18}\text{O}_{\text{PO}_4}$ values along the flow path and their significant positive correlation with $\delta^{18}\text{O}_{\text{H}_2\text{O}}$ ($R^2 = 0.44$; $p < 0.01$) (Fig. 4) suggest a pronounced influence of intracellular enzymatic cycling of P, resulting in an exchange of O atoms between PO₄ and ambient groundwater.

Fig. 1 | Groundwater sampling locations within the north-western Hetao Basin, Inner Mongolia Autonomous Region, PR China. The dark blue arrow shows the approximate groundwater flow direction from the Langshan Mountains in the north-west towards the flat plain in the centre of the Hetao Basin. Along the flow path, 13, 16, and 16 groundwater samples were collected in the alluvial fan (the blue circles), the transition area (the green circles) and the flat plain (the red circles), respectively. In particular, the bold circles show sampling locations of 12 groundwater samples that have been previously analyzed for 16S rRNA gene amplicon sequencing^{60,113,114}, including four samples in the alluvial fan (LY07, LY08, 17-7-11, and K2-6), four samples in the transition area (I-9, H01-30, I-3, and I-1), and four samples in the flat plain (K1-2, K1-6, I-16, and 1803). Maps created in Esri ArcMap 10.5 (ESRI World Image Basemap, source: Esri, Maxar, Earthstar Geographics).

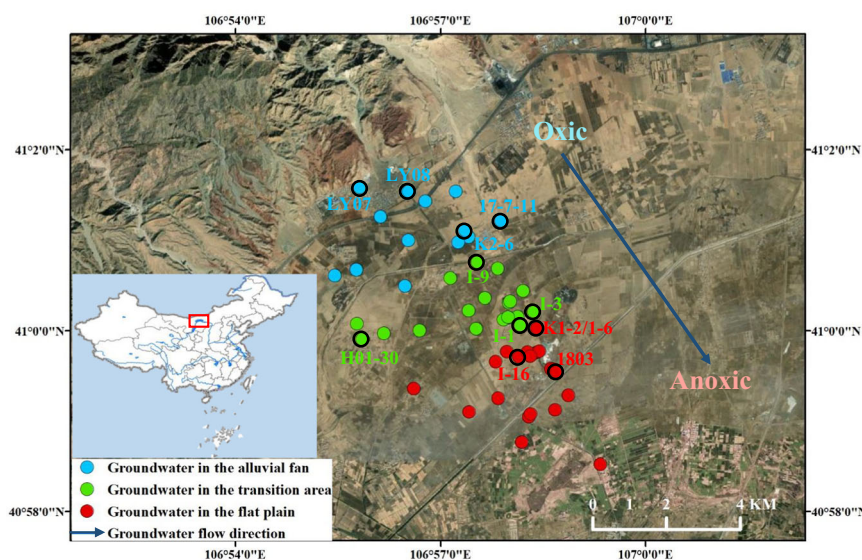
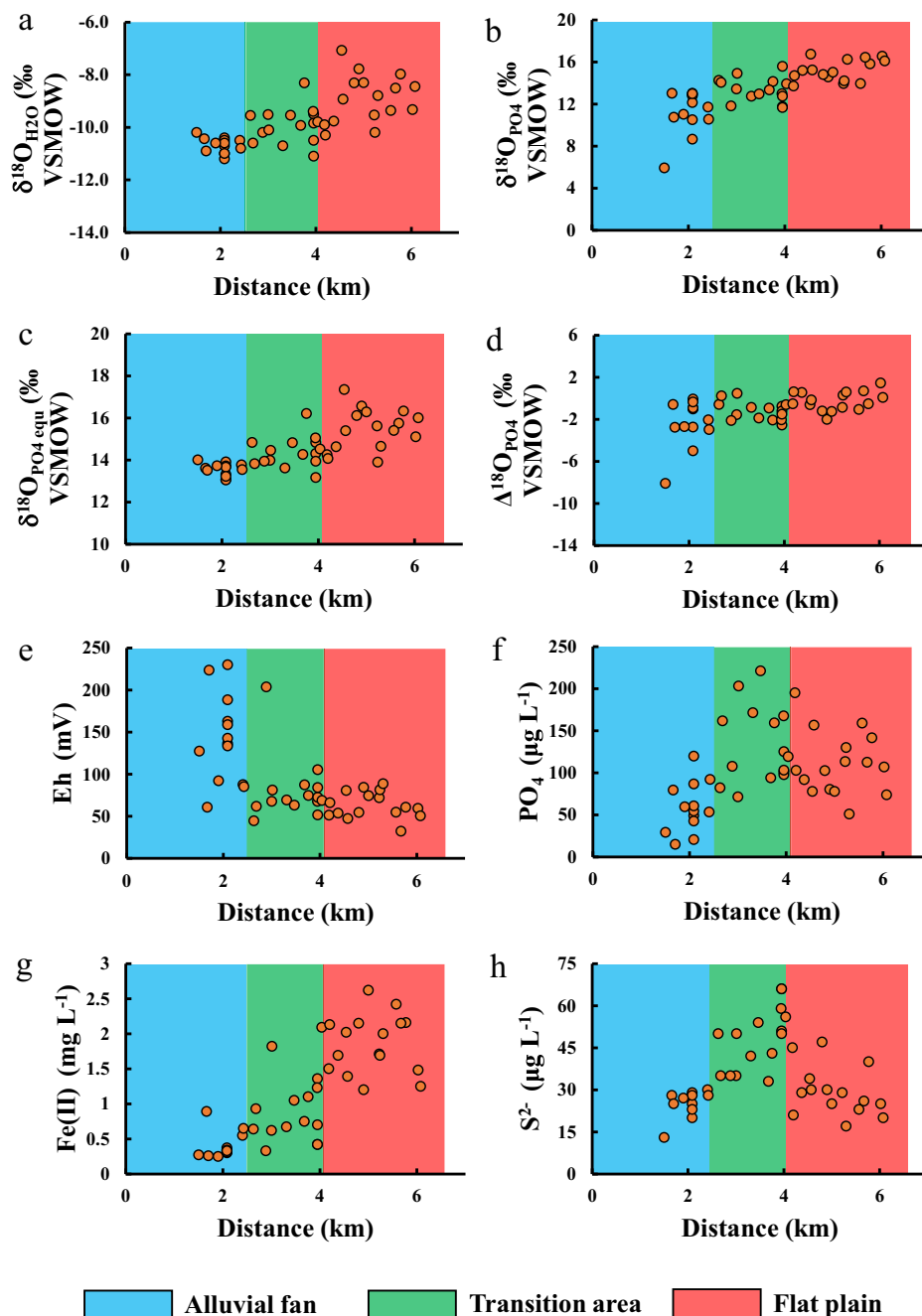


Fig. 2 | Spatial variation in groundwater $\delta^{18}\text{O}_{\text{PO}_4}$ values and redox-sensitive components along the flow path. a Observed $\delta^{18}\text{O}$ isotope values of groundwater ($\delta^{18}\text{O}_{\text{H}_2\text{O}}$). **b** Observed $\delta^{18}\text{O}$ isotope values of dissolved inorganic phosphate in groundwater ($\delta^{18}\text{O}_{\text{PO}_4}$). **c** Calculated theoretical equilibrium $\delta^{18}\text{O}_{\text{PO}_4}$ values of dissolved inorganic phosphate after intracellular microbial cycling ($\delta^{18}\text{O}_{\text{PO}_4 \text{ equ}}$). **d** Difference between observed $\delta^{18}\text{O}_{\text{PO}_4}$ and $\delta^{18}\text{O}_{\text{PO}_4 \text{ equ}}$ values ($\Delta^{18}\text{O}_{\text{PO}_4}$) (Negative $\Delta^{18}\text{O}_{\text{PO}_4}$ values indicate that observed $\delta^{18}\text{O}_{\text{PO}_4}$ were isotopically lighter (i.e. more ^{18}O -depleted) than the calculated equilibrium $\delta^{18}\text{O}_{\text{PO}_4 \text{ equ}}$ values). **e** Redox potential (Eh) of groundwater. **f–h** Concentrations of dissolved inorganic phosphate (PO_4), ferrous iron (Fe(II)), and sulfide (S^{2-}), respectively. The blue, green and red rectangles showed the ranges of the alluvial fan, the transition area and the flat plain, respectively. Results of statistical analyses are shown in Fig. 3.



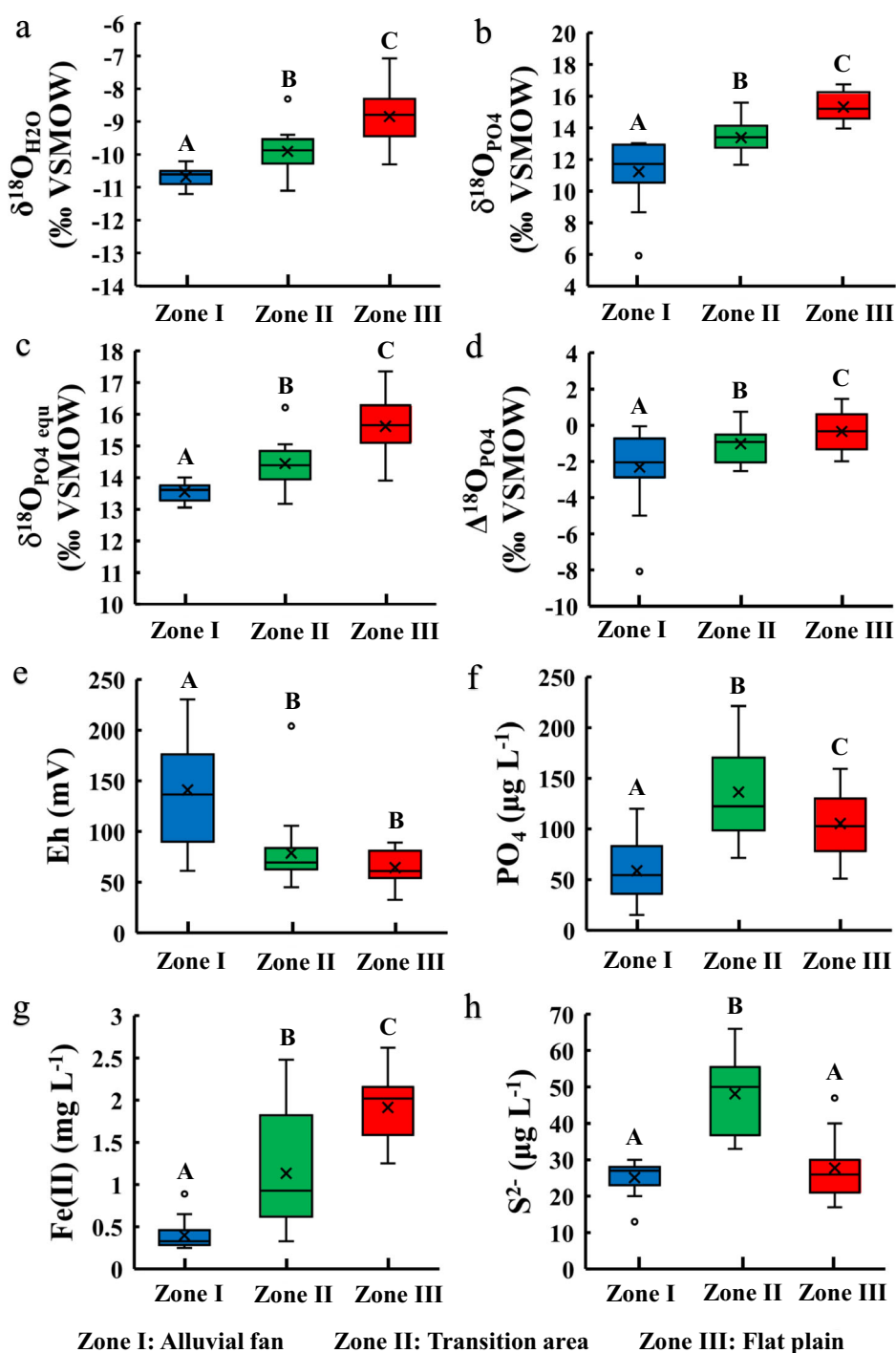
In natural ecosystems, the intracellular enzymatic cycling of PO_4 in microorganisms is associated with a temperature-dependent equilibrium isotope fractionation⁶⁵. In the study area, the groundwater temperatures showed only a small variation (10.9 ± 0.11 °C, see Supplementary Table S1). Based on Eq. (1) (see Data processing in Methods), we calculated the theoretical $\delta^{18}\text{O}_{\text{PO}_4 \text{ equ}}$ values that would be expected in the case of a complete overprinting by intracellular microbial PO_4 cycling⁵⁰. Our results showed that $\delta^{18}\text{O}_{\text{PO}_4 \text{ equ}}$ values significantly increased along the flow path (medians of +13.6‰, +14.4‰ and +15.6‰ in the alluvial fan, the transition area and the flat plain, respectively; Figs. 2c, 3c). More importantly, the difference between observed $\delta^{18}\text{O}_{\text{PO}_4}$ values and expected $\delta^{18}\text{O}_{\text{PO}_4 \text{ equ}}$ values ($\Delta^{18}\text{O}_{\text{PO}_4}$; see Eq. (2) in Methods) was relatively small, with a median value of less than -1 ‰ in the studied groundwater (Figs. 2d, 3d). This small difference suggests that O isotope ratios of dissolved PO_4 molecules in groundwater were significantly affected by microorganism intracellular cycling. Similarly, microbial PO_4 cycling was observed in other aquatic ecosystems, such as

marine sediments and lakes, as indicated by $\delta^{18}\text{O}_{\text{PO}_4}$ values close to $\delta^{18}\text{O}_{\text{PO}_4 \text{ equ}}$ values^{52,66}. Hence, microbial cycling of PO_4 also plays an important role in groundwater systems.

Increasing contribution of microbial cycling to dissolved PO_4 from oxic to anoxic conditions

Along the groundwater flow path, the Eh values sharply decreased from the alluvial fan (median of 137 mV) to the transition area (69.4 mV) and the flat plain (60.9 mV; Figs. 2e, 3e), indicating that the redox conditions of groundwater changed from oxic to anoxic. The median concentrations of dissolved PO_4 significantly ($p < 0.05$) increased from the alluvial fan ($51.0 \mu\text{g L}^{-1}$) to the transition area ($109 \mu\text{g L}^{-1}$) and the flat plain ($92.5 \mu\text{g L}^{-1}$; Figs. 2f, 3f), showing an increase of dissolved PO_4 concentrations under anoxic conditions. Furthermore, $\Delta^{18}\text{O}_{\text{PO}_4}$ values in groundwater significantly increased ($p < 0.01$) from the alluvial fan (median of -2.0 ‰), over the transition area (median of -1.1 ‰), to the flat plain

Fig. 3 | Statistical analyses on groundwater $\delta^{18}\text{O}_{\text{PO}_4}$ values and redox-sensitive components in the different zones. **a** Observed $\delta^{18}\text{O}$ isotope values of groundwater ($\delta^{18}\text{O}_{\text{H}_2\text{O}}$). **b** Observed $\delta^{18}\text{O}$ isotope values of dissolved inorganic phosphate in groundwater ($\delta^{18}\text{O}_{\text{PO}_4}$). **c** Calculated theoretical equilibrium $\delta^{18}\text{O}_{\text{PO}_4}$ values of dissolved inorganic phosphate after intensive intracellular microbial cycling ($\delta^{18}\text{O}_{\text{PO}_4 \text{ equ}}$). **d** Difference between $\delta^{18}\text{O}_{\text{PO}_4}$ and $\delta^{18}\text{O}_{\text{PO}_4 \text{ equ}}$ values ($\Delta^{18}\text{O}_{\text{PO}_4}$) (Negative $\Delta^{18}\text{O}_{\text{PO}_4}$ values indicate that observed $\delta^{18}\text{O}_{\text{PO}_4}$ were isotopically lighter (i.e. more ^{18}O -depleted) than the calculated equilibrium $\delta^{18}\text{O}_{\text{PO}_4 \text{ equ}}$ values). **e** Redox potential (Eh) of groundwater. **f–h** Concentrations of dissolved inorganic phosphate (PO_4), ferrous iron (Fe(II)), and sulfide (S^{2-}), respectively. The Zone I, II and III stand for the alluvial fan, the transition area and the flat plain, and are shown in blue, green, and red colours, respectively. Uppercase letters (A–C) indicate significant differences ($p < 0.05$) in measured variables among the three zones. $N = 13, 16,$ and 16 in the alluvial fan, the transition area, and the flat plain, respectively.



(median of -0.2‰), approaching zero (Figs. 2d, 3d). This indicated that the difference between observed $\delta^{18}\text{O}_{\text{PO}_4}$ values and expected $\delta^{18}\text{O}_{\text{PO}_4 \text{ equ}}$ values was getting smaller along the flow path. The significant negative correlation between $\Delta^{18}\text{O}_{\text{PO}_4}$ and Eh values ($r = -0.50$; $p < 0.01$; Fig. 5a) indicated an increasing contribution of microbial PO_4 cycling to the dissolved PO_4 along with the change from oxic to anoxic conditions. Hence, biogeochemical processes that are potentially associated with microbial PO_4 cycling and result in the changes of $\Delta^{18}\text{O}_{\text{PO}_4}$ values from oxic to anoxic conditions are discussed as following.

Microbial PO_4 cycling under oxic conditions

Although microbial PO_4 cycling contributed to the dissolved PO_4 , the largest $\Delta^{18}\text{O}_{\text{PO}_4}$ (median value of -2.0‰ ; Fig. 3d) and the most ^{18}O -depleted

isotope ratios of PO_4 in the alluvial fan suggest that $\delta^{18}\text{O}$ of dissolved PO_4 in groundwater under oxic conditions was closer to its source signal. Based on our previous investigation³⁷, either sedimentary organic matter (SOM) and/or apatite were considered as potential sources of PO_4 under oxic conditions in our groundwater system.

In the study area, SOM in aquifers is degradable⁶⁷ and mostly originates from buried plant residues in the unconsolidated sediments⁶⁸. Typical $\delta^{18}\text{O}_{\text{PO}_4}$ values of plants range from $+17\text{‰}$ to $+27\text{‰}$ ⁶⁹, which is reasonable to expect for the SOM as well. Previous experiments demonstrated that the extracellular P_{org} hydrolysis commonly occurs in two steps, which are catalyzed by phosphodiesterases (diesterases) and phosphomonoesterases (monoesterases), respectively⁴⁷. For each step, PO_4 inherits three O atoms from the P_{org} molecule and incorporates one O atom from ambient

water^{70,71}. Hence, PO₄ released from extracellular P_{org} hydrolysis contains signatures of both enzymatic steps and the combined isotopic effect of diesterase + monoesterase is expressed as Eq. (3)⁴⁷ (see Data processing in Methods). Considering the weakly alkaline pH of groundwater in the alluvial fan (pHs: 6.7 – 9.1; see Supplementary Table S1), alkaline phosphatase (APase) can be assumed to be the key extracellular monoesterase enzyme that was involved in OM degradation and the concomitant release of PO₄ to groundwater^{49,72}. In natural waters, PO₄ is expected to have a stronger RNA degradation signature than DNA degradation signature⁴⁷. For RNA, the fractionation factor between O incorporated into PO₄ and ambient water O is $-5(\pm 6)\text{‰}$ for the diesterase + APase pathway^{70,71}. Therefore, $\delta^{18}\text{O}_{\text{PO}_4}$ values of PO₄ from SOM biodegradation catalyzed by extracellular diesterase and APase enzymes would range from $+0.0\text{‰}$ to $+5.5\text{‰}$, shifting the observed $\delta^{18}\text{O}_{\text{PO}_4}$ values away from the $\delta^{18}\text{O}_{\text{PO}_4 \text{ equ}}$ values towards more ¹⁸O-depleted signatures^{22,69,73}. However, NH₄⁺ concentrations in groundwater of the alluvial fan were the lowest ($p < 0.05$)

among the three zones with median value of 0.40 mg L^{-1} (see Supplementary Table S1). In groundwater ecosystems, since NH₄⁺ mainly originates from the mineralization of N-containing OM⁵, NH₄⁺ represented a useful indicator of OM degradation^{74,75}. According to the lowest concentration of NH₄⁺, OM degradation played a less important role in PO₄ release in the alluvial fan as compared to the other two zones. This was in agreement with our previous investigations, demonstrating that when compared with the transition area and the flat plain, the bioreactivity of OM and the P_{org} contents in aquifer sediments of the alluvial fan were relatively lower^{35,37}. Hence, PO₄ released from OM degradation might not result in the largest $\Delta^{18}\text{O}_{\text{PO}_4}$ observed in the alluvial fan. Therefore, we infer a limited contribution of OM degradation to PO₄ concentrations in groundwater under oxic conditions.

In the aquifers, apatite dissolution is considered another source of dissolved PO₄^{37,76}. In the Hetao Basin, we found that Ca/Fe(II)-minerals represented the dominant sedimentary PO₄ pool and also that groundwater in the alluvial fan was undersaturated with regard to apatite³⁷. We further measured $\delta^{18}\text{O}_{\text{PO}_4}$ values of HCl-PO₄ (representing PO₄ in apatite minerals) in the aquifer sediments, which ranged from $+4.0\text{‰}$ to $+8.5\text{‰}$ (see Supplementary Table S2). The measured $\delta^{18}\text{O}$ values of HCl-PO₄ were in line with those previously reported for soils and sediments derived from igneous rocks (from $+5.3\text{‰}$ to $+9.0\text{‰}$)^{77,78}. In the adjacent Langshan Mountains, the contents of PO₄-P in metamorphic complex were reported to exceed 1000 mg kg^{-1} ⁷⁹. Notably, there were two groundwater samples with remarkably low $\delta^{18}\text{O}_{\text{PO}_4}$ values ($+5.9\text{‰}$ and $+8.7\text{‰}$) in the alluvial fan (Fig. 2b) that matched $\delta^{18}\text{O}_{\text{PO}_4}$ values of HCl-PO₄ in the sediments (from $+4.0\text{‰}$ to $+8.5\text{‰}$). This indicated that the release of PO₄ from igneous apatite dissolution characterized by low $\delta^{18}\text{O}_{\text{PO}_4}$ signals was the main process shifting $\delta^{18}\text{O}_{\text{PO}_4}$ values of groundwater away from isotopic equilibrium.

In the alluvial fan, the mean of observed $\delta^{18}\text{O}_{\text{PO}_4}$ values in groundwater was $+11.2\text{‰}$ (see Supplementary Table S1). Based on a simple two-end-member mixing model with the measured $\delta^{18}\text{O}_{\text{PO}_4}$ of igneous apatite (with $+4.0\text{‰}$ as lower and $+8.5\text{‰}$ as upper boundary) and the calculated $\delta^{18}\text{O}_{\text{PO}_4 \text{ equ}}$ of groundwater (mean value of $+13.6\text{‰}$ in the alluvial fan, see Supplementary Table S1), we estimated that 25–47% of the dissolved PO₄ was derived from igneous apatite dissolution. We therefore conclude that apatite dissolution contributed to the isotopic signal of PO₄ in groundwater under oxic conditions, whereas $> 53\%$ of the dissolved PO₄ was intensively turned over by microorganisms. Previous studies showed that in soil and

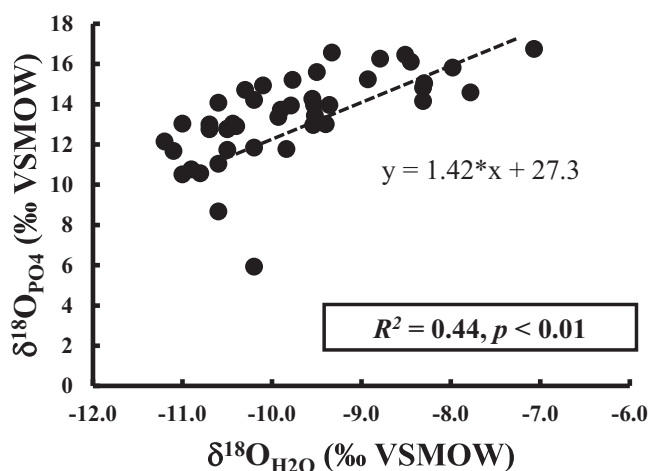


Fig. 4 | Relationship between observed $\delta^{18}\text{O}_{\text{PO}_4}$ and $\delta^{18}\text{O}_{\text{H}_2\text{O}}$ values in groundwater. $\delta^{18}\text{O}_{\text{PO}_4}$ values represent observed $\delta^{18}\text{O}$ isotope values of dissolved inorganic phosphate in groundwater; $\delta^{18}\text{O}_{\text{H}_2\text{O}}$ values represent observed $\delta^{18}\text{O}$ isotope values of groundwater. The regression coefficients (R^2) are provided together with the level of significance (p).

Fig. 5 | Relationship between $\Delta^{18}\text{O}_{\text{PO}_4}$ values and redox-sensitive components along the groundwater flow path. $\Delta^{18}\text{O}_{\text{PO}_4}$ values represent the isotope difference between observed $\delta^{18}\text{O}$ isotope values of dissolved inorganic phosphate in groundwater ($\delta^{18}\text{O}_{\text{PO}_4}$) and calculated theoretical equilibrium $\delta^{18}\text{O}_{\text{PO}_4}$ values of dissolved inorganic phosphate after intracellular microbial cycling ($\delta^{18}\text{O}_{\text{PO}_4 \text{ equ}}$). **a–d** $\Delta^{18}\text{O}_{\text{PO}_4}$ values against redox potential values (Eh), concentrations of dissolved ferrous iron (Fe(II)), dissolved inorganic phosphate (PO₄), and dissolved sulfide (S²⁻) in groundwater, respectively. The blue, green and red circles represent groundwater samples in the alluvial fan, the transition area and the flat plain, respectively. The correlation coefficients (r) are provided together with the level of significance (p).

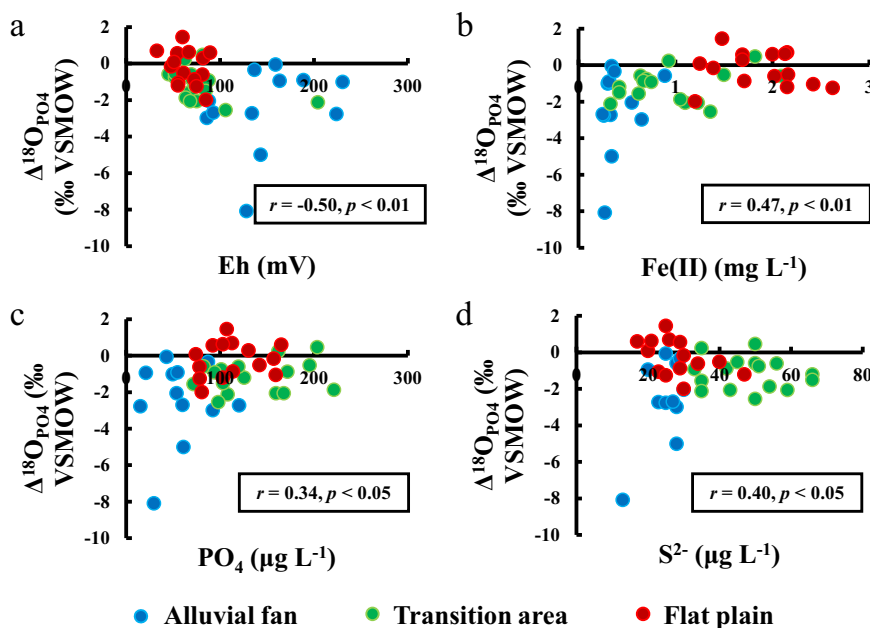
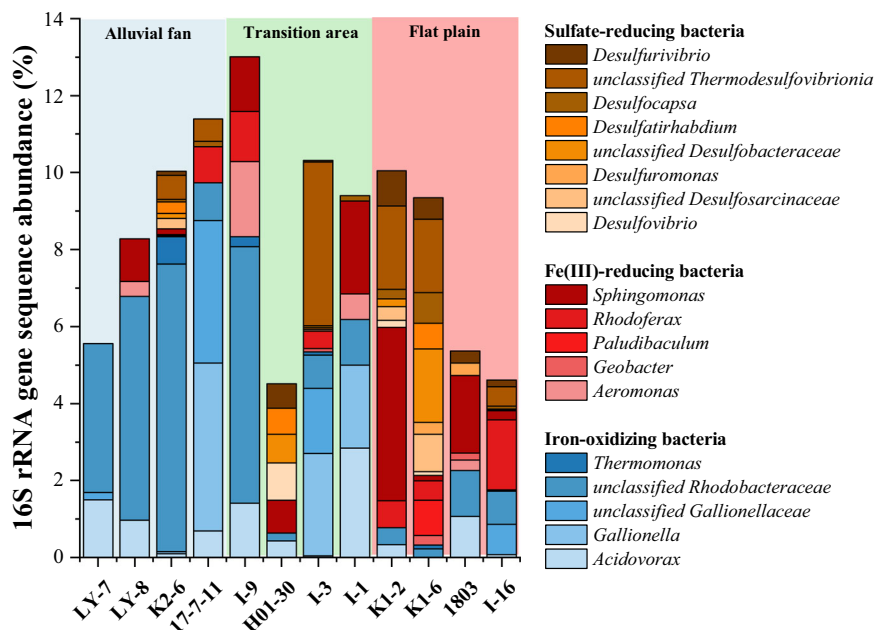


Fig. 6 | Microbial community composition along the groundwater flow path. From the alluvial fan to the flat plain, relative abundance of iron-oxidizing bacteria (bars in blue series) gradually decreased, while relative abundances of Fe(III)-reducing bacteria (bars in red series) and sulfate-reducing bacteria (bars in yellow series) gradually increased, showing a shift of microbial community from oxic to anoxic conditions.



marine environments, microbial activity and turnover releases PO_4 into solution under oxic conditions^{23,25,80,81}. Thus, our results highlight that dissolved PO_4 in oxic aquifers may be subject to active microbial cycling of PO_4 .

Microbial PO_4 cycling under anoxic conditions

As previously described, dissolved PO_4 was increased under anoxic conditions in the transition area and the flat plain. Along the groundwater flow path, Fe(II) concentrations significantly ($p < 0.01$) increased from the alluvial fan (0.33 mg L^{-1} in median) over the transition area (0.84 mg L^{-1} in median) to the flat plain (1.94 mg L^{-1} in median) (Figs. 2g, 3g). Since Fe(III) oxides represent a potential source for PO_4 in the aquifer sediments from the basin (average: 9.10 mg kg^{-1})³⁷, the positive correlation between groundwater Fe(II) and PO_4 ($r = 0.53$, $p < 0.01$) suggests that the reductive dissolution of Fe(III) oxides was an important process of PO_4 mobilization and resulted in the high concentrations of dissolved PO_4 under anoxic conditions. Simultaneously, the $\Delta^{18}\text{O}_{\text{PO}_4}$ values gradually increased along the groundwater flow path, approaching zero (Fig. 3d). Especially in the flat plain, the median $\Delta^{18}\text{O}_{\text{PO}_4}$ value was not significantly different from zero ($p > 0.05$), reflecting that O isotope equilibration was reached between the dissolved PO_4 and ambient groundwater. Hence, under anoxic conditions, it appears that the isotopic signal of the dissolved PO_4 mostly originates from microbial cycling. There are two possible explanations for the observed changes of $\Delta^{18}\text{O}_{\text{PO}_4}$ value along the flow path. One is that more PO_4 with an equilibrium $\delta^{18}\text{O}_{\text{PO}_4}$ value was released into groundwater via the reductive dissolution of Fe(III) oxides under anoxic conditions, and the other is that dissolved PO_4 was more intensively cycled by microorganisms in groundwater of the flat plain.

Regarding the first explanation, it would require that PO_4 associated with Fe(III) oxides attained an isotopic equilibrium value before and/or during the reductive dissolution of Fe(III) oxides. We cannot exactly determine the time when the microorganism left their isotope imprint on Fe(III)-associated PO_4 . Some studies showed that in a thermally stratified Archean ocean, Fe(III)-associated PO_4 recorded equilibrium $\delta^{18}\text{O}_{\text{PO}_4}$ values with cooler ocean surface waters⁵². Moreover, studies on Fe(III) oxide deposits from both Red and Green seamounts located near the East Pacific Rise (EPR) concluded that PO_4 bound to Fe(III) oxides was intensively cycled by Fe-oxidizing bacteria as evidenced by mineral morphology and $\delta^{18}\text{O}_{\text{PO}_4}$ values of PO_4 in Fe(III) oxides⁵⁴. Specifically, Fe(III) oxides in both seamounts were mainly composed of twisted filaments, stalks, and hollow sheaths that resembled the characteristic remains of the Fe-oxidizing bacteria *Gallionella ferruginea* and *Leptothrix*⁸². In the study area, Fe-oxidizing

bacteria were identified and dominated in groundwater of the alluvial fan with an averaged relative abundance of 7.6%, including *Gallionella*⁸³, *Acidovorax*⁸⁴, *Thermomonas*⁸⁵, an unclassified member of the Gallionellaceae family and an unclassified member of the Rhodobacteraceae⁸⁶ family (Fig. 6). Moreover, the enriched functional genes of *foxEY*, *Cyc1* and *sulfocyanin* were observed in the alluvial fan, further indicating that microbial Fe oxidation was the major Fe-related biogeochemical process⁸⁷. Hence, microbial imprint might have happened before the reductive dissolution of Fe(III) oxides, and therefore PO_4 associated with Fe(III) oxides attained an equilibrium value under oxic conditions. In this case, if PO_4 was later released via the reductive dissolution of Fe(III) oxides without further microbial imprint, we expect that $\delta^{18}\text{O}_{\text{PO}_4}$ values in groundwater under anoxic conditions were similar to $\delta^{18}\text{O}_{\text{PO}_4 \text{ equ}}$ values under oxic conditions. However, as we observed, $\delta^{18}\text{O}_{\text{PO}_4}$ values in the flat plain under anoxic conditions (+14.0‰ - +16.7‰) were significantly higher than $\delta^{18}\text{O}_{\text{PO}_4 \text{ equ}}$ values in the alluvial fan under oxic conditions (+13.1‰ - +14.0‰) (see Supplementary Table S1), which suggest that microbial imprint on PO_4 associated with Fe(III) oxides was further generated under anoxic conditions. This was consistent with the findings that both dissolved PO_4 in porewater and Fe(III) oxide-associated PO_4 in anoxic bottom sediments in the Chesapeake Bay had $\delta^{18}\text{O}_{\text{PO}_4}$ values near equilibrium values⁸⁸, and that the release of PO_4 from Fe(III)/Al oxides in lake sediments under anaerobic conditions led to high PO_4 concentrations in Lake Shijiuhu in the Yangtze River Basin, with biotic activity regulating the $\delta^{18}\text{O}_{\text{PO}_4}$ values toward equilibrium⁴¹.

When redox conditions gradually changed from oxic to anoxic along the groundwater flow path, Fe(III)-reducing bacteria became the dominant microorganism that utilized PO_4 associated with Fe(III) oxides. This was evidenced by the higher abundance of Fe(III)-reducing bacteria in the flat plain (Fig. 6), including *Aeromonas*⁸⁹, *Geobacter*⁹⁰, *Paludibaculum*⁹¹, *Rhodiferax*⁹² and *Sphingomonas*⁹³. Along the flow path, the relative abundance of those dominant Fe(III)-reducing bacteria remarkably increased from the alluvial fan (0.7% in average), over the transition area (2.3% in average), to the flat plain (2.9% in average) (Fig. 6). Furthermore, Xiu et al.⁸⁷ found that the enriched functional gene of *omcS* was present in the same flat plain with the abundance of 0.6 fragments per kilobase per million mapped fragments (FPKM), indicating microbial Fe(III) reduction became the major Fe-cycling process. Previous experiments showed that a significant fraction of Fe(III) oxides-bound PO_4 was bioavailable and was taken up by bacteria attaining an isotopic equilibrium composition⁵³. Moreover, it is well-known that Fe(III)-reducing bacteria can access solid Fe(III) as electron

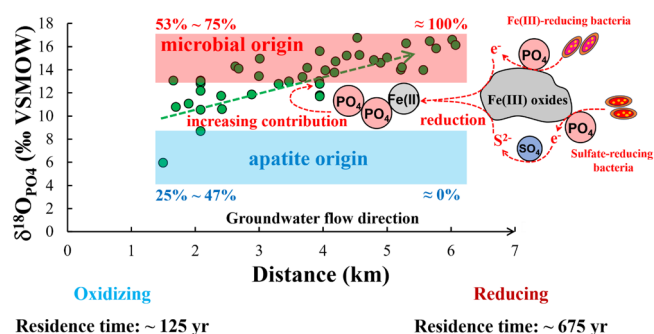


Fig. 7 | Conceptual figure of the increasing contribution of microbial cycling to dissolved inorganic phosphate (PO₄) from oxic to anoxic conditions in flood-plain aquifers of the Hetao Basin. The green points show the observed $\delta^{18}\text{O}_{\text{PO}_4}$ isotopic value of PO₄ ($\delta^{18}\text{O}_{\text{PO}_4}$) in groundwater. The red rectangle stands for the range of equilibrium $\delta^{18}\text{O}_{\text{PO}_4}$ values after intracellular microbial cycling. The blue rectangle represents the range of $\delta^{18}\text{O}_{\text{PO}_4}$ values of igneous apatite. Along the flow path, the redox conditions gradually changed from oxic to anoxic, and the groundwater residence time increased from about 125 yr to 675 yr. Under these conditions, the green dashed line shows an increasing trend of $\delta^{18}\text{O}_{\text{PO}_4}$ values towards equilibrium $\delta^{18}\text{O}_{\text{PO}_4}$ values along the groundwater flow path, indicating an increasing contribution of microbial cycling to dissolved PO₄ from 53% – 75% to nearly 100%. This is probably due to the release of PO₄ with an equilibrium $\delta^{18}\text{O}_{\text{PO}_4}$ value from Fe(III) oxides, as a result of Fe(III) reduction in the presence of Fe(III)- and sulfate-reducing bacteria (red dashed lines). Moreover, the increasing residence times of groundwater allow the dissolved PO₄ to be more microbially cycled and consequently the groundwater $\delta^{18}\text{O}_{\text{PO}_4}$ values gradually approached isotopic equilibrium.

acceptor, inducing the reductive dissolution of Fe(III) oxides via multiple electron transfer strategies⁹⁴. As we observed, along the groundwater flow path, Fe(II) concentrations and $\Delta^{18}\text{O}_{\text{PO}_4}$ value consistently increased with a significantly positive correlation ($r = 0.47$, $p < 0.01$; Fig. 5b). Simultaneously, the concentrations of PO₄ also increased with $\Delta^{18}\text{O}_{\text{PO}_4}$ value with a positive correlation ($r = 0.34$, $p < 0.05$; Fig. 5c). The significant positive correlations between $\Delta^{18}\text{O}_{\text{PO}_4}$ value and dissolved Fe(II), and PO₄ suggest that more PO₄ with an equilibrium $\delta^{18}\text{O}_{\text{PO}_4}$ value was released into groundwater via the reductive dissolution of Fe(III) oxides, as a result of increasing microbial Fe(III) reduction under anoxic conditions in the flat plain (Fig. 7). Similarly, Zhao et al. observed that a shift of $\delta^{18}\text{O}_{\text{PO}_4}$ towards equilibrium at a depth around 140 m below the seafloor in the Peru Margin upwelling zone corresponded well with a shift in microbial communities⁴⁴.

Under anoxic conditions, microbial sulfate reduction would further promote the reductive dissolution of Fe(III) oxides with attendant release of PO₄ with an equilibrium $\delta^{18}\text{O}_{\text{PO}_4}$ value into groundwater. Similar to Fe(III)-reducing bacteria, sulfate-reducing bacteria also utilized PO₄ associated with Fe(III) oxides under anoxic conditions. This is evidenced by the presence of available sulfate (median of 225 mg L⁻¹), and sulfate-reducing bacteria (Fig. 6) (including *Desulfovibrio*⁹⁵, *Desulfuromonas*⁹⁶, *Desulfatirhabdium*⁹⁷, an unclassified member of the Desulfosarcinaceae⁹⁵ family, and an unclassified member of the Desulfobacteraceae⁹⁵ family) in groundwater of the transition area and the flat plain. Specifically, the averaged relative abundance of those dominant sulfate-reducing bacteria increased from the alluvial fan (0.2%), over the transition area (0.6%), to the flat plain (1.3%) (Fig. 6). In addition, in our previous study⁸⁷, the enriched functional genes related to dissimilatory sulfate reduction (average FPKM from 0.4 to 1.1), such as *sat*, *APR*, *aprAB*, and *dsrAB*, were observed in groundwater of the same transition area and flat plain. As shown in Figs. 2h and 3h, the concentrations of S²⁻ in the transition area (median of 50.0 $\mu\text{g L}^{-1}$) were significantly higher than those in the alluvial fan (median of 25.0 $\mu\text{g L}^{-1}$), which indicated that microbial sulfate reduction occurred in groundwater under anoxic conditions. Both S²⁻ and Fe(II) increased from the alluvial fan to the transition area with a positive correlation ($r = 0.57$, $p < 0.01$), suggesting that the reductive dissolution of Fe(III) oxides was promoted by microbial sulfate reduction, probably via the oxidation of produced S²⁻⁹⁸ and/or electron

shuttling of produced sulfur intermediates⁹⁴ (Fig. 7). In the study area, bacteria capable of disproportionating intermediate sulphur species was also detected in groundwater of the transition area and the flat plain with relative abundance of 1.6%, including *Desulfocapsa*⁹⁹, *Desulfurivibrio*¹⁰⁰, and an unclassified member of Thermodesulfobionia¹⁰¹ family. Moreover, sulfur and oxygen isotope analyses confirmed that both sulfide and sulfur intermediates (i.e., elemental sulfur) produced from microbial sulfate reduction reduced the Fe(III) oxides¹⁰². Hence, the positive correlation between S²⁻ and $\Delta^{18}\text{O}_{\text{PO}_4}$ values ($r = 0.40$, $p < 0.05$; Fig. 5d) indicated that more PO₄ with an equilibrium $\delta^{18}\text{O}_{\text{PO}_4}$ value was released into groundwater via the reductive dissolution of Fe(III) oxides, as a result of increasing microbial sulfate reduction under anoxic conditions (Fig. 7). Notably, both the concentrations of S²⁻ and PO₄ decreased from the transition area to the flat plain (Fig. 3f, h). This was possibly due to the precipitation of ferrous sulfide minerals, such as pyrite¹⁰³, and subsequent PO₄ adsorption¹⁰⁴. In the flat plain, pyrite was oversaturated in groundwater³⁷ and observed in aquifer sediments¹⁰³. Since previous experiments demonstrated a negligible isotopic fractionation between dissolved and adsorbed PO₄ during the abiotic process of PO₄ adsorption on Fe-minerals at long reaction time (> 100 h)⁶⁴, we do not expect a shift in $\delta^{18}\text{O}_{\text{PO}_4}$ signals by PO₄ adsorption on ferrous sulfide minerals in this study.

In addition, the increase in $\Delta^{18}\text{O}_{\text{PO}_4}$ value towards zero from the alluvial to the flat plain was related to the increasing groundwater residence time along the flow path during which dissolved PO₄ in groundwater was more intensively cycled by microorganisms. In the study area, the average groundwater flow rates gradually decrease from 20 m yr⁻¹ in the alluvial fan, over 10 m yr⁻¹ in the transition area, to 5 m yr⁻¹ in the flat plain¹⁰⁵. Accordingly, we estimated that the mean residence times of groundwater in the alluvial fan area (around 2.5 km-length), in the transition area (around 1.5 km-length), and in the flat plain area (around 2 km-length) were 125 years, 275 years, and 675 years, respectively. During these long groundwater residence times, the abiotic oxygen isotopic exchange between dissolved PO₄ and ambient groundwater should be discussed. Previous studies predicted that the half-life for a complete abiotic equilibrium exchange between PO₄ and water would be 88,000 yrs at 10 °C^{44,106}, which was close to groundwater temperature in the study area (11.3 °C on average; see Supplementary Table S1). The predicted time was much longer than the groundwater residence time in the study area. Therefore, along the flow path, the changes of $\Delta^{18}\text{O}_{\text{PO}_4}$ values more likely resulted from microbially-mediated isotopic exchange. The longer residence time of groundwater allowed the dissolved PO₄ to be more microbially cycled and consequently the $\delta^{18}\text{O}_{\text{PO}_4}$ values of groundwater gradually increased towards isotopic equilibrium. This was in line with previous studies, demonstrating that the long residence time in the lower catchments of the Yasu River (Japan) and the Redon River (France) fostered biological PO₄ recycling and the equilibration of $\delta^{18}\text{O}$ values of dissolved PO₄^{39,40}.

Methods

Study area

The study area is located in the northwest of the Hetao Basin in the Inner Mongolia Autonomous Region, PR China (Fig. 1), between the Langshan Mountains and the Yellow River. The Quaternary sediments that fill the basin have both alluvial and lacustrine sources, which are mainly derived from the metamorphic complex of the Langshan Mountains and partly from fluvial deposits of the Yellow River^{61,62}. There are two clay layers that are enriched in organic matter at the depths of approximately 5 m and 40 m below land surface (bls), overlying two sandy and silty aquifers and preventing vertical filtration⁶¹. Groundwater flows from the Langshan Mountains in the north-west in a south-eastern direction towards the centre of the Hetao Basin. Here, hydraulic conductivity decreases from about 9.0 m d⁻¹ near the mountains to 3.8 m d⁻¹ in the centre of the floodplain⁷⁹.

Along the groundwater flow, there is a typical hydrogeochemical zonation in the aquifers. In the alluvial fan near the mountains, the aquifers consist of pluvial-alluvial sediments, whereas the aquifer sediments in the flat plain are mainly composed of inland lacustrine sediments⁶¹. A transition

area was identified between the alluvial fan and the flat plain, which is characterized by mixed-source sediment deposits⁶². In the aquifer sediments of the study area, high PO₄ contents were mostly found in clay/silty clay layers, whilst PO₄ contents in sand/silt layers were comparatively low. Ca/Fe(II)-minerals represented the dominant sedimentary PO₄ pool of total extractable PO₄, followed by exchangeable PO₄, PO₄ in Fe(III) oxides, strongly adsorbed PO₄ to metal-(oxyhydr)oxides and residual PO₄³⁷. Moreover, along the groundwater flow path, P_{org} contents were obviously higher in the sediments of the flat plain than in the sediments of the alluvial fan³⁷. Based on our previous investigation at the same site, the average groundwater flow rates gradually decrease from 20 m yr⁻¹ in the alluvial fan, over 10 m yr⁻¹ in the transition area, to 5 m yr⁻¹ in the flat plain¹⁰⁵. From the alluvial fan to the flat plain, distinct redox reactions occur with the sequence of O₂-reduction, NO₃-reduction, Mn(VI)-reduction, As(V)-reduction, Fe(III)-reduction and SO₄²⁻-reduction⁵⁹. Representative microbial communities that catalyze those redox reactions were also detected, including *Gallionella* (Fe(II)-oxidizer), *Pseudomonas* (denitrifier), *Rhodoferrax* (Fe(III)-reducer), *Bacillus* (As(V)-reducer) and *Desulfatiferula* (sulphate-reducer)⁶⁰.

Groundwater sampling and field analysis

Along the groundwater flow path, 45 groundwater samples, including 13 samples from the alluvial fan, 16 samples from the transition area, and 16 samples from the flat plain, were collected from the irrigation wells with depths of 10–100 m bls in July 2019 (Fig. 1). For data evaluation, groundwater samples from shallow and deep aquifers were pooled for the respective zones. Based on the previous investigation, the spatial variations of physiochemical groundwater parameters, including PO₄ concentrations³⁷, showed no significant difference ($p > 0.05$) between the two aquifers along the groundwater flow path. Hence, we did not differentiate the shallow and deep aquifers in this study.

Before sampling, wells were pumped for more than 20 min until sensitive parameters, including groundwater temperature (T), electrical conductivity (EC), pH, oxidation reduction potential (ORP), which was converted into Eh after corrected to the standard hydrogen electrode provided in the manual of HANNA, HI 9828), and dissolved oxygen (DO) of groundwater were stable. All samples used for laboratory analysis were filtered through 0.45 µm membrane filters (cellulose nitrate filters, Jinteng), with the exception of samples used for dissolved organic carbon (DOC), which were filtered through 0.45 µm syringe filters (PTFE filters, Jinteng). All bottles and flasks for sample storage were acid-washed and preconditioned before use. Details on groundwater sampling and field analysis please see Supplementary Note 1.

For groundwater δ¹⁸O_{PO₄} analysis, a volume of 1–3 L of fresh groundwater was collected in polyethylene bottles to obtain sufficient PO₄ for the isotopic analysis (around 1 mg in total), depending on the PO₄ concentrations measured in the field (ascorbic acid; PhosVer3; Hach, DR2800). To isolate PO₄ from groundwater, we added 1–3 g of FeSO₄ (Sigma-Aldrich, ACS reagent, ≥ 99.0%) into the groundwater to advance the coprecipitation of PO₄ by Fe(III)-oxides after 24 h of aeration¹⁰⁷. The precipitates were filtered and air-dried, and then stored in sterile polythene bottles for further laboratory analysis. Phosphate concentrations in filtrates were analyzed after the filtration to make sure that PO₄ in groundwater was completely removed by the co-precipitation with Fe(III)-oxides. Results showed that PO₄ concentrations in filtrates taken after co-precipitation and filtration remained below the detection limit (5 µg L⁻¹ for UV-VIS spectrophotometer [Varian Cary 100] based on the molybdenum blue method¹⁰⁸), indicating a successful separation of PO₄ from groundwater.

Sediment sampling and PO₄ extraction

Two boreholes were both drilled with depths between 10 and 80 m below the land surface (bls). Specifically, borehole K2 was located in the alluvial fan area near the mountains, while borehole K1 was located in the flat plain. Four sediment samples were collected from each borehole with increasing depths (see Supplementary Table S2). After taken out, sediment samples

were immediately sealed in foil and in sterile bags flushed with ultrapure nitrogen gas. Before the laboratory PO₄ extraction and δ¹⁸O_{PO₄} analysis, samples were preserved in a refrigerator at –80 °C.

To differentiate PO₄ originating from microbial cycling and from dissolution of primary minerals, we targeted the PO₄ in apatite minerals^{109,110}. In order to extract HCl-PO₄, we first used NaOH solution to remove labile P (including exchangeable P, adsorbed P onto Fe/Mn-(oxyhydr)oxides and structurally bound P in Al-(oxyhydr)oxides)⁷. Then, HCl-PO₄ in sediments was extracted by 1 M HCl solution (Sigma-Aldrich, p.a. ≥ 37 %)³⁷. According to previous studies, PO₄ extracted by HCl solution could mainly contain three different sedimentary P pools, including Fe(III) oxides-bound PO₄, detrital apatite and authigenic apatite^{44,111,112}. Prior to HCl-PO₄ extraction, we had checked the presence of Fe(III) oxides-bound PO₄ by the extraction of citrate-dithionite-bicarbonate (CDB) solution³⁷. The results showed that Fe(III) oxides-bound PO₄ (average content: 9.62 ± 2.65 mg kg⁻¹; n = 8) only accounted for a negligible proportion (about 4%) if it was co-extracted with HCl-PO₄ (average content: 242 ± 24.7 mg kg⁻¹; n = 8). Moreover, adsorbed PO₄ onto Fe(III)-(oxyhydr)oxides was removed by NaOH solution⁷. Hence, HCl-PO₄ in this study mainly represented sedimentary P pool of apatite minerals, including detrital apatite and authigenic apatite. Details on extraction of HCl-PO₄ from sediments please see Supplementary Note 2.

Laboratory analysis

Stable oxygen isotope ratio analyses of PO₄ (δ¹⁸O_{PO₄}) were carried out using groundwater and sediment samples from the Hetao Basin. Prior to the δ¹⁸O_{PO₄} analyses of groundwater samples and extracted HCl-PO₄ from sediments, a multistep purification procedure was modified based on the protocols developed by Tamburini et al.¹¹⁰ and Neidhardt et al.¹⁵. In brief, this procedure consists of multiple dissolution, precipitation, and resin sorption steps to remove all other possible O-bearing compounds and constituents that would interfere with the isotopic analysis (see Supplementary Fig. S1). According to our previous investigation in the Hetao Basin, the average concentrations of dissolved PO₄ and dissolved P_{org} in groundwater were 82.4 and 6.2 µg L⁻¹, respectively, which suggested that dissolved P in groundwater mainly presents in the form of PO₄. Moreover, P_{org} components in the sediments mostly preserves in the exchangeable P pool³⁷, which was removed by NaOH solution prior to HCl extraction. Hence, the isotopic effect on δ¹⁸O_{PO₄} analyses of groundwater and HCl-extractable PO₄ by means of P_{org} hydrolysis is considered negligible in this study. Details on the laboratory analyses of groundwater major cations, anions, dissolved P species, DOC, and oxygen and hydrogen isotopes (δ¹⁸O_{H₂O} and δ²H_{H₂O}) please see Supplementary Note 3.

For PO₄ purification from groundwater, the Fe(III)-(hydr)oxide precipitates were dissolved in 50 mL 16.5% HNO₃ to release co-precipitated PO₄ and the filters were rinsed with Millipore water to completely remove PO₄. The extracted HCl-PO₄ from sediments were preserved in 50 mL 1 M HCl solutions. Then, the protocol basically followed the method from reference 110, which consisted of two precipitation steps (see Supplementary Fig. S1). First, PO₄ was precipitated in the form of ammonium-phospho-molybdate (APM, (NH₄)₃PMo₁₂O₄₀) by adding 25 mL 35% NH₄NO₃ solution (Roth) and 40 mL 10% ammonium molybdate solution ((NH₄)₆Mo₇O₂₄·4H₂O) (Roth, 99%) and placing in a warm bath at 20 °C. After filtration (0.22 µm PES membrane; Millipore Express, Merck) and rinsing with Millipore water, the APM precipitate was dissolved in 25 mL ammonium-citrate solution. The next precipitation step was then induced by adding 25 mL acidic magnesia solution and 6 mL NH₄OH/H₂O (1:1 v/v) solution in order to keep the pH between 8 and 9. Magnesium-ammonium-phosphate (MAP, NH₄MgPO₄·6H₂O) crystals form while stirring overnight. After filtration (0.22 µm PES membrane; Millipore Express, Merck) and rinsing, MAP crystals were dissolved by adding 20 mL 0.5 M HNO₃. After dissolution, possible interfering cations were removed by shaking the samples together with 6 mL cation exchange resin slurry (BioRad, AG[®] 50W-X8, H+ form) overnight. Resin and sample solution were then separated by filtration (0.22 µm PES membrane; Millipore Express, Merck).

Afterwards, 4 mL 2 M AgNO₃ was added to the sample solution to remove chloride as AgCl precipitate to assure the purity of the final Ag₃PO₄ precipitate. Sample solutions were filtered (0.2 µm GTTP membrane; Isopore, Merck) again and then transferred to new 50 mL tubes. Finally, the PO₄ was precipitated as Ag₃PO₄ following the addition of 5 mL silver ammine solution and the placement of the open tubes into an oven at 50 °C for 48 h. The δ¹⁸O_{PO₄} of groundwater and HCl-PO₄ from sediments was then analysed in form of pure Ag₃PO₄ by TC/EA-IRMS (PYRO cube and Iso-Prime100, Elementar Analysensysteme, Germany) in a continuous flow mode. The isotope analysis was carried out in the laboratory of Soil Science and Geoecology at the University of Tübingen. All δ¹⁸O_{PO₄} values were reported in the conventional per mil notation (‰) relative to the Vienna Standard Mean Ocean Water (VSMOW) reference standard.

For internal calibration and quality control of groundwater δ¹⁸O_{PO₄} measurements, three certified international reference standards (USGS80, δ¹⁸O_{PO₄} = +13.1‰; USGS81, δ¹⁸O_{PO₄} = +35.4‰; IAEA602, δ¹⁸O = +71.3‰) were included in each TC/EA IRMS run. Within the sample weight range of 0.1–0.7 mg, the standard error (SE) of the repeatedly measured δ¹⁸O_{PO₄} values of the three reference standards were ± 0.07‰ (USGS80; *n* = 20), ± 0.26‰ (USGS81; *n* = 18), and ± 0.97‰ (IAEA602; *n* = 8), respectively (see Supplementary Table S3). The differences between the average measured δ¹⁸O_{PO₄} values and certified values of the three reference standards were +0.2‰, −0.8‰, and +0.3‰, respectively (see Supplementary Table S3). Notably, the measured δ¹⁸O_{PO₄} values of USGS80, which were the closest to those of the groundwater δ¹⁸O_{PO₄} values, showed the smallest SE and the smallest difference between average values and certified values (see Supplementary Fig. S2a), reflecting a good stability and accuracy of the isotope analyses. All samples were analyzed as triplicates and within the same weight range as to the reference standards, except when the Ag₃PO₄ mass was too low. The oxygen yield was checked by comparing the weights of Ag₃PO₄ introduced into TC/EA-IRMS and the obtained CO peak area⁵⁰. The purity of the precipitated Ag₃PO₄ was ensured by the close match of two regression lines representing the standards and the samples (see Supplementary Fig. S2b). Moreover, possible effects of arsenic contamination on the δ¹⁸O_{PO₄} values were considered¹⁵. Results showed that arsenic was mostly removed from the samples through the procedure, with the effects on δ¹⁸O_{PO₄} values being less than 1‰ (see Supplementary Table S4). The δ¹⁸O_{PO₄} measurements of HCl-PO₄ extracted from sediments were also calibrated by two internal standards (USGS80, δ¹⁸O_{PO₄} = +13.1‰; USGS81, δ¹⁸O_{PO₄} = +35.4‰) and the quality was controlled by an additional external standard (IAEA601, δ¹⁸O = +23.1‰). Three certified standards were included in each TC/EA IRMS run and the results also showed a good accuracy and reproducibility for all reference materials (see Supplementary Table S5).

Pure solid KH₂PO₄ salt (Roth, ≥ 99.0%) was dissolved and included as an internal quality control in each sample batch. Mass balance results showed that after the purification, an average of 89.3 ± 0.3% (*n* = 4) of the initial PO₄ was converted into Ag₃PO₄ precipitate. The δ¹⁸O_{PO₄} value of the processed internal standard shifted approximately 0.35‰ VSMOW (average: +13.98 ± 0.12‰, *n* = 12) when compared to that of the pure initial KH₂PO₄ salt (average: +13.63 ± 0.14‰, *n* = 3). Thus, the internal standard demonstrated that PO₄ loss and oxygen fractionation during the purification were insignificant (see Supplementary Tables S6 and S7). Further details regarding the quality of the δ¹⁸O_{PO₄} analyses of groundwater and sedimentary HCl-PO₄ please see Supplementary Fig. S2 and Tables S3–S7.

16S rRNA gene analysis

At the study site, 12 groundwater samples used for the δ¹⁸O_{PO₄} analyses in this study have been previously analyzed for 16S rRNA gene amplicon sequencing^{60,113,114}. They include 4 samples in the alluvial fan, 4 samples in the transition area and 4 samples in the flat plain. For all those 16S rRNA gene analyses at the study site, DNA was extracted from each sample using the same FastDNA SPIN Kit for Soil (MP Biotechnology, Solon, OH, USA) and the 16S rRNA gene was amplified from the genomic DNA using the same primers 338 F (ACTCCTACGGGAGGCAGCAG) and 806 R

(GGACTACHVGGGTWTCTAAT) targeting the V3-V4 region^{60,113,114}. In this study, raw FASTQ files containing results of 16S rRNA gene sequencing were collected from those previous studies. Then, the sequences were imported into QIIME2 v2023.5¹¹⁵ and processed with DADA2¹¹⁶, including trimming, quality-filtering and demultiplexing. The remaining sequences were clustered into operational taxonomic units (OTUs) at the 97% sequence identity level. Finally, the taxonomic assignment of each OTUs was conducted using Naïve Bayes classifier algorithm trained on data from SILVA v.138.1. The clean data for each sample were uploaded to the NCBI database under the accession number PRJNA1082075. More details regarding the DNA extraction and high-throughput sequencing please refer to Xiu et al.⁶⁰, Ke et al.¹¹³ and Wang¹¹⁴.

Data processing

Microbial PO₄ turnover that is catalyzed by intracellular enzymes (i.e., pyrophosphatases) leads to an exchange of O atoms between PO₄ and ambient water (groundwater in our case) associated with a temperature-dependent equilibrium fractionation⁶⁵. The resulting theoretical equilibrium value of δ¹⁸O_{PO₄} (δ¹⁸O_{PO₄equ}) after microbial PO₄ turnover can be calculated based on known temperature (*T*) and stable oxygen isotope value of ambient water (δ¹⁸O_{H₂O})¹⁰⁷. In the study area, despite the relatively long residence times of groundwater (~ 100 yr ~ 1200 yr¹⁰⁵) (see Study area in Methods), the relatively fast intracellular isotope fractionation can reach equilibrium within several days⁵⁰, which is why we assume that measured groundwater δ¹⁸O_{H₂O} and temperatures were representative for the calculation of δ¹⁸O_{PO₄equ}. Recently, the equation was revised by ref. 50, and we rearranged the δ¹⁸O_{PO₄equ} calculation as Eq. (1).

$$\delta^{18}\text{O}_{\text{PO}_4\text{equ}} = (\delta^{18}\text{O}_{\text{H}_2\text{O}} + 1000) * e^{(14.43 * 1000 / T[\text{K}] - 26.54) / 1000} - 1000 \quad (1)$$

An isotopic shift of measured values of δ¹⁸O_{PO₄} from the theoretical equilibrium value of δ¹⁸O_{PO₄equ} (Δ¹⁸O_{PO₄}) is defined as Eq. (2)⁴⁹.

$$\Delta^{18}\text{O}_{\text{PO}_4} = \delta^{18}\text{O}_{\text{PO}_4} - \delta^{18}\text{O}_{\text{PO}_4\text{equ}} \quad (2)$$

Based on the observed δ¹⁸O_{PO₄} and calculated δ¹⁸O_{PO₄equ} in groundwater, a simple two-end member mixing model was applied in this study to calculate the contribution of microbial cycling to dissolved PO₄ in the aquifers, relative to other abiotic processes that release PO₄ with specific O isotope values.

Extracellular P_{org} hydrolysis is catalyzed by enzymes and occurs in two steps, including (1) hydrolytic cleavage of phosphodiester (P-diester) bonds that results in the generation of phosphomonoesters (P-monoesters) and (2) conversion of P-monoesters to an organic group plus PO₄⁴⁷. The first step is catalyzed by phosphodiesterase (diesterase) and the second step is catalyzed by phosphomonoesterase (monoesterase)⁴⁷. For each step, PO₄ inherits three atoms from the P_{org} molecule and incorporates one O atom from ambient water^{70,71}. Hence, PO₄ released from extracellular P_{org} hydrolysis contains signatures of both enzymatic steps and the combined isotopic effect of diesterase + monoesterase is expressed as Eq. (3):

$$\delta^{18}\text{O}_{\text{PO}_4} = 0.5 * \delta^{18}\text{O}_{\text{org}} + 0.5 * (\delta^{18}\text{O}_{\text{water}} + F) \quad (3)$$

where δ¹⁸O_{org} stands for the original stable oxygen isotope value of organophosphorus compounds and *F* is the combined fractionation factor associated with breaking diester and monoester bonds ($F = (F_1 + F_2) / 2$)⁴⁷. In natural waters, PO₄ is expected to have a stronger RNA degradation signature than DNA degradation signature⁴⁷. For RNA, the fractionation factor between O incorporated into PO₄ and ambient water O is −5 (± 6)‰ for the diesterase + alkaline phosphatase (APase) pathway ($F_1 = +20$ ‰; $F_2 = -30$ ‰)^{70,71}.

Along the groundwater flow path, distributions of δ¹⁸O_{PO₄} values and redox components in the three zones were analyzed by SPSS Statistics (Vers. 25) using group comparisons. The data were first checked for normal distribution using the Shapiro-Wilk test. Based on the outcome, group means

of variables in different zones were compared by a one-way ANOVA, or a non-parametric Kruskal-Wallis one-way ANOVA on ranks and by a pairwise post-hoc test (LSD) with Bonferroni correction. The group means of $\Delta^{18}\text{O}_{\text{PO}_4}$ in different zones were compared with zero by a one-sample t-test. Moreover, two-tailed Spearman correlation tests and ordinary least squares regression analysis were applied to examine the relationships between the measured variables. In addition, we evaluated the residuals of selected regressions. The confidence interval for all tests was set to 95% and p -values ≤ 0.05 were considered statistically significant.

Reporting summary

Further information on research design is available in the Nature Portfolio Reporting Summary linked to this article.

Data availability

Data supporting the findings of this study are available in the Mendeley open repository with the identifier <https://doi.org/10.17632/2crfxdydfwb.1>¹⁷. Sequencing data for 16S rRNA has been deposited in the NCBI Sequence Read Archive under the BioProject ID: PRJNA1082075.

Received: 12 September 2023; Accepted: 30 August 2024;

Published online: 10 September 2024

References

- Holman, I. P. et al. Phosphorus in groundwater—an overlooked contributor to eutrophication? *Hydrol. Process.* **22**, 5121–5127 (2008).
- Lewandowski, J., Meinikmann, K., Nützmann, G. & Rosenberry, D. O. Groundwater – the disregarded component in lake water and nutrient budgets. Part 2: effects of groundwater on nutrients. *Hydrol. Process.* **29**, 2922–2955 (2015).
- Kazmierczak, J. et al. Groundwater-controlled phosphorus release and transport from sandy aquifer into lake. *Limnol. Oceanogr.* **9999**, 1–17 (2020).
- Meinikmann, K., Hupfer, M. & Lewandowski, J. Phosphorus in groundwater discharge—A potential source for lake eutrophication. *J. Hydrol.* **524**, 214–226 (2015).
- Yu, L. et al. Groundwater impacts on surface water quality and nutrient loads in lowland polder catchments: monitoring the greater Amsterdam area. *Hydrol. Earth Syst. Sci.* **22**, 487–508 (2018).
- Biswas, A. et al. Role of competing ions in the mobilization of arsenic in groundwater of Bengal Basin: insight from surface complexation modeling. *Water Res.* **55**, 30–39 (2014).
- Neidhardt, H. et al. Phosphate immobilisation dynamics and interaction with arsenic sorption at redox transition zones in floodplain aquifers: Insights from the Red River Delta, Vietnam. *J. Hazard. Mater.* **411**, 125128 (2021).
- Guo, H. M., Wen, D. G., Liu, Z. Y., Jia, Y. F. & Guo, Q. A review of high arsenic groundwater in mainland and Taiwan, China: distribution, characteristics and geochemical processes. *Appl. Geochem.* **41**, 196–217 (2014).
- Warrack, J., Kang, M., Sperber, C. & von Groundwater phosphorus concentrations: global trends and links with agricultural and oil and gas activities. *Environ. Res. Lett.* **17**, 014014 (2021).
- Chen, X. M., Wo, F., Chen, C. & Fang, K. Seasonal changes in the concentrations of nitrogen and phosphorus in farmland drainage and groundwater of the Taihu Lake region of China. *Environ. Monit. Assess.* **169**, 159–168 (2010).
- McGinley, P. M., Masarik, K. C., Gotkowitz, M. B. & Mechenich, D. J. Impact of anthropogenic geochemical change and aquifer geology on groundwater phosphorus concentrations. *Appl. Geochem.* **72**, 1–9 (2016).
- Parkhurst, D. L., Stollenwerk, K. G. & Colman, J. A. Reactive-Transport Simulation of Phosphorus in the Sewage Plume at the Massachusetts Military Reservation, Cape Cod, Massachusetts. *U.S. Geological Survey Water-Resources Investigations Report.* **4017**, 40 (2003).
- Spiteri, C. et al. Modelling the geochemical fate and transport of wastewater-derived phosphorus in contrasting groundwater systems. *J. Contam. Hydrol.* **92**, 87–108 (2007).
- Roy, J. W. & Bickerton, G. Elevated dissolved phosphorus in riparian groundwater along gaining urban streams. *Environ. Sci. Technol.* **48**, 1492–1498 (2014).
- Neidhardt, H. et al. Biogeochemical phosphorus cycling in groundwater ecosystems—Insights from South and Southeast Asian floodplain and delta aquifer. *Sci. Total Environ.* **644**, 1357–1370 (2018).
- Dubrovsky, N. M. et al. The Quality of Our Nation’s Waters—Nutrients in the Nation’s Streams and Groundwater, 1992–2004. *US Geological Survey Circular* **1350**, 174 (2010).
- Kazmierczak, J. et al. Transport of geogenic phosphorus to a groundwater-dominated eutrophic lake. *J. Hydrol.* **598**, 126175 (2021).
- Ioka, S. et al. Species and potential sources of phosphorus in groundwater in and around Mataram City, Lombok Island, Indonesia. *SN Appl. Sci.* **3**, 27 (2021).
- Bi, P., Huang, G. X., Liu, C. Y. & Li, L. P. Geochemical factors controlling natural background levels of phosphate in various groundwater units in a large-scale urbanized area. *J. Hydrol.* **608**, 127594 (2022).
- Tao, Y. Q. et al. Carbon and iron isotope approach elucidates the enrichment of geogenic phosphorus in alluvial-lacustrine sedimentary aquifers. *J. Hydrol.* **607**, 127517 (2022).
- Davies, C. L., SurrIDGE, B. W. J. & Goody, D. C. Phosphate oxygen isotopes within aquatic ecosystems: global data synthesis and future research priorities. *Sci. Total Environ.* **496**, 563–575 (2014).
- Colman, A. S., Blake, R. E., Karl, D. M., Fogel, M. L. & Turekian, K. K. Marine phosphate oxygen isotopes and organic matter remineralization in the oceans. *Proc. Natl. Acad. Sci. USA.* **102**, 13023–13028 (2005).
- Goldhammer, T. et al. Phosphate oxygen isotopes: Insights into sedimentary phosphorus cycling from the Benguela upwelling system. *Geochim. Cosmochim. Acta.* **75**, 3741–3756 (2011).
- Bi, Q. F. et al. The microbial cycling of phosphorus on long-term fertilized soil: Insights from phosphate oxygen isotope ratios. *Chem. Geol.* **483**, 56–64 (2018).
- Bauke, S. L. et al. Phosphate oxygen isotope ratios in vegetated riparian buffer strip soils. *Vadose Zone J.* **21**, e20193 (2022).
- Granger, S. J. et al. The oxygen isotopic composition of phosphate in river water and its potential sources in the Upper River Taw catchment, UK. *Sci. Total Environ.* **574**, 680–690 (2017).
- Xiu, W. et al. Understanding active biogeochemical As-mobilizing processes in the inland Hetao Basin: insight from DNA-based (bulk) and RNA-based (active) microbial community. *Environ. Sci. Technol.* **55**, 15181–15195 (2021).
- Hall, S. J., Treffkorn, J. & Silver, W. L. Breaking the enzymatic latch: impacts of reducing conditions on hydrolytic enzyme activity in tropical forest soils. *Ecology.* **95**, 2964–2973 (2014).
- Gross, A., Pett-Ridge, J. & Silver, W. J. Soil oxygen limits microbial phosphorus utilization in humid tropical forest soils. *Soil Systems.* **2**, 65 (2018).
- Jilbert, T. et al. Beyond the Fe-P-redox connection: preferential regeneration of phosphorus from organic matter as a key control on Baltic Sea nutrient cycles. *Biogeosciences.* **8**, 1699–1702 (2011).
- Gross, A., Lin, Y., Weber, P. K., Pett-Ridge, J. & Silver, W. L. The role of soil redox conditions in microbial phosphorus cycling in humid tropical forests. *Ecology.* **101**, e02928 (2020).
- Hall, S. J. & Silver, W. L. Reducing conditions, reactive metals, and their interactions can explain spatial patterns of surface soil carbon in a humid tropical forest. *Biogeochemistry.* **125**, 149–165 (2015).

33. Peretyazhko, T. & Sposito, G. Iron(III) reduction and phosphorous solubilization in humid tropical forest soils. *Geochim. Cosmochim. Acta.* **69**, 3643–3652 (2005).
34. Lin, Y. et al. Phosphorus fractionation responds to dynamic redox conditions in a humid tropical forest soil. *J. Geophys. Res.-Biogeo.* **123**, 3016–3027 (2018).
35. Zhou, Y. Z. et al. Characteristics and implication of stable carbon isotope in high arsenic groundwater systems in the northwest Hetao Basin, Inner Mongolia, China. *J. Asian Earth Sci.* **163**, 70–79 (2018).
36. Yan, L. et al. Organic-matter composition and microbial communities as key indicators for arsenic mobility in groundwater aquifers: Evidence from PLFA and 3D fluorescence. *J. Hydrol.* **591**, 125308 (2020).
37. Li, Y. et al. Spatial variation in dissolved phosphorus and interactions with arsenic in response to changing redox conditions in floodplain aquifers of the Hetao Basin, Inner Mongolia. *Water Res.* **209**, 117930 (2022).
38. Li, Q. et al. Tracing the sources of phosphorus along the salinity gradient in a coastal estuary using multi-isotope proxies. *Sci. Total Environ.* **792**, 148353 (2021).
39. Ishida, T. et al. Identification of Phosphorus Sources in a Watershed Using a Phosphate Oxygen Isoscape Approach. *Environ. Sci. Technol.* **53**, 4707–4716 (2019).
40. Pistocchi, C. et al. Tracing the sources and cycling of phosphorus in river sediments using oxygen isotopes: Methodological adaptations and first results from a case study in France. *Water Res.* **111**, 346–356 (2017).
41. Yuan, H. Z. et al. Tracing the sources of phosphorus in lake at watershed scale using phosphate oxygen isotope ($\delta^{18}\text{O}_\text{P}$). *Chemosphere.* **305**, 135382 (2022).
42. Stout, L. M., Joshi, S. R., Kana, T. M. & Jaisi, D. P. Microbial activities and phosphorus cycling: an application of oxygen isotope ratios in phosphate. *Geochim. Cosmochim. Acta.* **138**, 101–116 (2014).
43. Wang, Y. et al. Phosphate oxygen isotope fingerprints of past biological activity in the Atacama Desert. *Geochim. Cosmochim. Acta.* **311**, 1–11 (2021).
44. Zhao, M. Y. et al. Oxygen isotopic fingerprints on the phosphorus cycle within the deep subseafloor biosphere. *Geochim. Cosmochim. Acta.* **310**, 169–186 (2021).
45. Blake, R. E., O'Neil, J. R. & Garcia, G. A. Oxygen isotope systematics of biologically mediated reactions of phosphate: 1. Microbial degradation of organophosphorus compounds. *Geochim. Cosmochim. Acta.* **61**, 4411–4422 (1997).
46. O'Neil, J. R., Vennemann, T. W. & McKenzie, W. F. Effects of speciation on equilibrium fractionations and rates of oxygen isotope exchange between $(\text{PO}_4)_\text{(aq)}$ and H_2O . *Geochim. Cosmochim. Acta.* **67**, 3135 (2003).
47. Liang, Y. H. & Blake, R. E. Compound- and enzyme-specific phosphodiester hydrolysis mechanisms revealed by $\delta^{18}\text{O}$ of dissolved inorganic phosphate: Implications for marine P cycling. *Geochim. Cosmochim. Acta.* **73**, 3782–3794 (2009).
48. Von Sperber, C., Kries, H., Tamburini, F., Bernasconi, S. M. & Frossard, E. The effect of phosphomonoesterases on the oxygen isotope composition of phosphate. *Geochim. Cosmochim. Acta.* **125**, 519–527 (2014).
49. Blake, R. E., O'Neil, J. R. & Surkov, A. V. Biogeochemical cycling of phosphorus: insights from oxygen isotope effects of phosphoenzymes. *Am. J. Sci.* **305**, 596–620 (2005).
50. Chang, S. J. & Blake, R. E. Precise calibration of equilibrium oxygen isotope fractionations between dissolved phosphate and water from 3 to 37 °C. *Geochim. Cosmochim. Acta.* **150**, 314–329 (2015).
51. Chang, S. J., Blake, R. E. & Colman, A. S. Oxygen isotope exchange rates between phosphate and water catalyzed by inorganic pyrophosphatase: Implications for the biogeochemical cycle of phosphorus. *Earth Planet. Sci. Lett.* **570**, 117071 (2021).
52. Blake, R. E., Chang, S. J. & Lepland, A. Phosphate isotope evidence for a temperate and biologically active Archean ocean. *Nature.* **464**, 1029–1032 (2010).
53. Jaisi, D. P., Kukkadapu, R. K., Stout, L. M., Varga, T. & Blake, R. E. Biotic and abiotic pathways of phosphorus cycling in minerals and sediments: Insights from oxygen isotope ratios in phosphate. *Environ. Sci. Technol.* **45**, 6254–6261 (2011).
54. Blake, R. E., Alt, J. C. & Martini, A. M. Oxygen isotope ratios of PO_4 : an inorganic indicator of enzymatic activity and P metabolism and a new biomarker in the search for life. *Proc. Natl. Acad. Sci. USA* **98**, 2148 (2001).
55. Young, M. B. et al. Characterizing the oxygen isotopic composition of phosphate sources to aquatic ecosystems. *Environ. Sci. Technol.* **43**, 5190 (2009).
56. Guo, H. M. et al. Pathways of coupled arsenic and iron cycling in high arsenic groundwater of the Hetao basin, Inner Mongolia, China: an iron isotope approach. *Geochim. Cosmochim. Acta.* **112**, 130–145 (2013).
57. Guo, H. M. et al. Contrasting distributions of groundwater arsenic and uranium in the western Hetao basin, Inner Mongolia: Implications for origins and fate controls. *Sci. Total Environ.* **541**, 1172–1190 (2016).
58. Guo, H. M. et al. Hydrogeological and biogeochemical constrains of arsenic mobilization in shallow aquifers from the Hetao basin, Inner Mongolia. *Environ. Pollut.* **159**, 876–883 (2011).
59. Jia, Y. F., Guo, H. M., Jiang, Y. X., Wu, Y. & Zhou, Y. Z. Hydrogeochemical zonation and its implication for arsenic mobilization in deep groundwaters near alluvial fans in the Hetao Basin, Inner Mongolia. *J. Hydrol.* **518**, 410–420 (2014).
60. Xiu, W. et al. Linking microbial community composition to hydrogeochemistry in the western Hetao Basin: Potential importance of ammonium as an electron donor during arsenic mobilization. *Environ. Int.* **136**, 105489 (2020).
61. Shi, J. S. et al. Investigation and evaluation report on groundwater resources and environmental problems in the Hetao Basin (in Chinese). *National Geological Archives of China.* **136148**, 770 (2014).
62. Guo, H. M., Yang, S. Z., Tang, X. H., Li, Y. & Shen, Z. L. Groundwater geochemistry and its implications for arsenic mobilization in shallow aquifers of the hetao basin, Inner Mongolia. *Sci. Total Environ.* **393**, 131–144 (2008).
63. Liang, Y. & Blake, R. E. Oxygen isotope fractionation between apatite and aqueous-phase phosphate: 20–45 °C. *Chem. Geol.* **238**, 121–133 (2007).
64. Jaisi, D. P., Blake, R. E. & Kukkadapu, R. K. Fractionation of oxygen isotopes in phosphate during its interactions with iron oxides. *Geochim. Cosmochim. Acta.* **74**, 1309–1319 (2010).
65. Longinelli, A. & Nuti, S. Revised phosphate-water isotopic temperature scale. *Earth Planet. Sci. Lett.* **19**, 373–376 (1973).
66. Elsbury, K. E. et al. Using oxygen isotope of phosphate to trace phosphorus sources and cycling in Lake Erie. *Environ. Sci. Technol.* **43**, 3108–3114 (2009).
67. Qiao, W. et al. Molecular Evidence of Arsenic Mobility Linked to Biodegradable Organic Matter. *Environ. Sci. Technol.* **54**, 7280–7290 (2020).
68. Mao, R. Y. et al. Characteristics and compound-specific carbon isotope of sedimentary lipids in high arsenic aquifers in the Hetao basin, Inner Mongolia. *Environ. Pollut.* **241**, 85–95 (2018).
69. Tamburini, F., Pistocchi, C., Helfenstein, J. & Frossard, E. A method to analyse the isotopic composition of oxygen associated with organic phosphorus in soil and plant material. *Eur. J. Soil Sci.* **69**, 816–826 (2018).
70. Liang, Y. & Blake, R. E. Oxygen isotope composition of phosphate in organic compounds: isotope effects of extraction methods. *Org. Geochem.* **37**, 1263–1277 (2006).
71. Liang, Y. & Blake, R. E. Oxygen isotope signature of Pi regeneration from organic compounds by phosphomonoesterases and photooxidation. *Geochim. Cosmochim. Acta.* **70**, 3957–3969 (2006).

72. Ayuso, S. V., Guerrero, M. C., Montes, C. & López-Archilla, A. I. Regulation and Spatiotemporal patterns of extracellular enzyme activities in a coastal, sandy aquifer system (Donana, SW Spain). *Microb. Ecol.* **62**, 162–176 (2011).
73. Angert, A., Weiner, T., Mazeh, S. & Sternberg, M. Soil phosphate stable oxygen isotopes across rainfall and bedrock gradients. *Environ. Sci. Technol.* **46**, 2156–2162 (2012).
74. Du, Y. et al. Enrichment of geogenic ammonium in Quaternary alluvial-lacustrine aquifer systems: evidence from carbon isotopes and DOM characteristics. *Environ. Sci. Technol.* **54**, 6104–6114 (2020).
75. Rivett, M. O., Buss, S. R., Morgan, P., Smith, J. W. N. & Bemment, C. D. Nitrate attenuation in groundwater: A review of biogeochemical controlling processes. *Water Res.* **42**, 4215–4232 (2008).
76. Bingham, S. T. et al. Rates of hydroxyapatite formation and dissolution in a sandstone aquifer: Implications for understanding dynamic phosphate behaviour within an agricultural catchment. *Appl. Geochem.* **115**, 114034 (2020).
77. Tamburini, F., Pfahler, V., von Sperber, C., Frossard, E. & Bernasconi, S. M. Oxygen Isotopes for Unraveling Phosphorus Transformations in the Soil-Plant System: A Review. *Soil Sci. Soc. Am. J.* **78**, 38–46 (2014).
78. Burmann, F. et al. The source of phosphate in the oxidation zone of ore deposits: evidence from oxygen isotope compositions of pyromorphite. *Geochim. Cosmochim. Acta.* **123**, 427–439 (2013).
79. Guo, H. M. et al. Contrasting distributions of groundwater arsenic and uranium in the Hetao basin, Inner Mongolia: Implication for origins and fate controls. *Sci. Total Environ.* **541**, 1172–1190 (2016).
80. Hacker, N., Wilcke, W. & Oelmann, Y. The oxygen isotope composition of bioavailable phosphate in soil reflects the oxygen isotope composition in soil water driven by plant diversity effects on evaporation. *Geochim. Cosmochim. Acta.* **248**, 387–399 (2019).
81. Helfenstein, J. et al. Combining spectroscopic and isotopic techniques gives a dynamic view of phosphorus cycling in soil. *Nat. Commun.* **9**, 3226 (2018).
82. Alt, J. C. Hydrothermal oxide and nontronite deposits on seamounts in the eastern Pacific. *Marine Geol.* **81**, 227–239 (1988).
83. de Vet, W. W. J. M., Dinkla, I. J. T., Rietveld, L. C. & van Loosdrecht, M. C. M. Biological iron oxidation by *Gallionella* spp. in drinking water production under fully aerated conditions. *Water Res.* **45**, 5389–5398 (2011).
84. Huang, G. Y. et al. Cadmium immobilization during nitrate-reducing Fe(II) oxidation by *Acidovorax* sp. BoFeN1: Contribution of bacterial cells and secondary minerals. *Chem. Geol.* **639**, 121729 (2023).
85. Pan, Y. et al. Microbial mixotrophic denitrification using iron(II) as an assisted electron donor. *Water Res.* **X**, 19, 100176 (2023).
86. Tian, T. et al. Exclusive microbially driven autotrophic iron-dependent denitrification in a reactor inoculated with activated sludge. *Water Res.* **170**, 115300 (2020).
87. Xiu, W. et al. Genome-resolved metagenomic analysis of groundwater: Insights into arsenic mobilization in biogeochemical interaction networks. *Environ. Sci. Technol.* **56**, 10105–10119 (2022).
88. Joshi, S. R. et al. Organic matter remineralization predominates phosphorus cycling in the Mid-Bay sediments in the Chesapeake Bay. *Environ. Sci. Technol.* **49**, 5887–5896 (2015).
89. Shi, Z. J. et al. Hexavalent chromium removal by a new composite system of dissimilatory iron reduction bacteria *Aeromonas hydrophila* and nanoscale zero-valent iron. *Chem. Eng. J.* **362**, 63–70 (2019).
90. Cutting, R. S., Coker, V. S., Fellowes, J. W., Lloyd, J. R. & Vaughan, D. J. Mineralogical and morphological constraints on the reduction of Fe(III) minerals by *Geobacter sulfurreducens*. *Geochim. Cosmochim. Acta.* **73**, 4004–4022 (2009).
91. Dedysh, S. N., Beletsky, A. V., Kulichevskaya, I. S., Mardanov, A. V. & Ravin, N. V. Complete genome sequence of *Paludibaculum fermentans* P105T, a facultatively anaerobic acidobacterium capable of dissimilatory Fe(III) reduction. *Microbial Resour. Announc.* **10**, e01313–e01320 (2021).
92. Finneran, K. T., Johnsen, C. V. & Lovley, D. R. *Rhodoferrax ferrireducens* sp. nov., a psychrotolerant, facultatively anaerobic bacterium that oxidizes acetate with the reduction of Fe(III). *Int. J. Syst. Evol. Microbiol.* **53**, 669–673 (2003).
93. Ding, J., Zhang, Y. B., Quan, X. & Chen, S. Anaerobic biodecolorization of AO7 by a newly isolated Fe(III)-reducing bacterium *Sphingomonas* strain DJ. *J. Chem. Technol. Biotechnol.* **90**, 158–165 (2015).
94. Kappler, A. et al. An evolving view on biogeochemical cycling of iron. *Nat. Rev. Microbiol.* **19**, 360–374 (2021).
95. Dar, S. A., Yao, L., van Dongen, U., Kuenen, J. G. & Muyzer, G. Analysis of diversity and activity of sulfate-reducing bacterial communities in sulfidogenic bioreactors using 16S rRNA and *dsrB* genes as molecular markers. *Appl. Environ. Microbiol.* **73**, 594–604 (2007).
96. Guo, Y. et al. Complete genome sequence of *Desulfuromonas* sp. Strain AOP6, an iron(III) reducer isolated from subsurface sediment. *Microbial Resour. Announc.* **9**, e01325–19 (2020).
97. Mardanov, A. V. et al. Sulfate-reducing bacteria in the microbial community of acidic drainage from a gold deposit tailing storage. *Microbiology.* **86**, 286–288 (2017).
98. Kocar, B. D., Borch, T. & Fendorf, S. Arsenic Repartitioning during Biogenic Sulfidization and Transformation of Ferrihydrite. *Geochim. Cosmochim. Acta.* **74**, 980–994 (2010).
99. Böttcher, M. E., Thamdrup, B. & Vennemann, T. W. Oxygen and sulfur isotope fractionation during anaerobic bacterial disproportionation of elemental sulfur. *Geochim. Cosmochim. Acta.* **65**, 1601–1609 (2001).
100. Sorokin, D. Y., Tourova, T. P., Mußmann, M. & Muyzer, G. *Dethiobacter alkaliphilus* gen. nov. sp. nov., and *Desulfurivibrio alkaliphilus* gen. nov. sp. nov.: two novel representatives of reductive sulfur cycle from soda lakes. *Extremophiles.* **12**, 431–439 (2008).
101. Umezawa, K., Kojima, H., Kato, Y. & Fukui, M. *Dissulfurispira thermophila* gen. nov., sp. nov., a thermophilic chemolithoautotroph growing by sulfur disproportionation and proposal of novel taxa in the phylum *Nitrospirota* to reclassify the genus *Thermodesulfovibrio*. *Syst. Appl. Microbiology.* **44**, 126184 (2021).
102. Guo, H. M. et al. Sulfur cycling-related biogeochemical processes of arsenic mobilization in the Western Hetao Basin, China: evidence from multiple isotope approaches. *Environ. Sci. Technol.* **50**, 12650–12659 (2016).
103. Wang, H. Y. et al. Arsenic sequestration in pyrite and greigite in the buried peat of As-contaminated aquifers. *Geochim. Cosmochim. Acta.* **284**, 107–119 (2020).
104. Han, Y. S., Park, J. H., Min, Y. & Lim, D. H. Competitive adsorption between phosphate and arsenic in soil containing iron sulfide: XAS experiment and DFT calculation approaches. *Chem. Eng. J.* **397**, 125426 (2020).
105. Gao, Z. P., Jia, Y. F., Guo, H. M., Zhang, D. & Zhao, B. Quantifying geochemical processes of arsenic mobility in groundwater from an inland basin using a reactive transport model. *Water Resour. Res.* **56**, e2019WR025492 (2020).
106. Lecuyer, C., Grandjean, P. & Sheppard, S. M. F. Oxygen isotope exchange between dissolved phosphate and water at temperatures <135°C: Inorganic versus biological fractionations. *Geochim. Cosmochim. Acta.* **63**, 855–862 (1999).
107. Gruau, G. et al. The oxygen isotope composition of dissolved anthropogenic phosphates: a new tool for eutrophication research? *Water Res.* **39**, 232–238 (2005).
108. Nagul, E. A., McKelvie, I. D., Worsfold, P. & Kolev, S. D. The molybdenum blue reaction for the determination of orthophosphate revisited: opening the black box. *Anal. Chim. Acta.* **890**, 60–82 (2015).
109. Polain, K. et al. Determination of Agricultural Impact on Soil Microbial Activity Using $\delta^{18}\text{O}_{\text{P-HCl}}$ and Respiration Experiments. *ACS Earth Space Chem.* **2**, 683–691 (2018).
110. Tamburini, F., Bernasconi, S. M., Angert, A., Weiner, T. & Frossard, E. A method for the analysis of the $\delta^{18}\text{O}$ of inorganic phosphate extracted from soils with HCl. *Eur. J. Soil Sci.* **61**, 1025–1032 (2010).

111. Anderson, L. D. & Delaney, M. L. Sequential extraction and analysis of phosphorus in marine sediments: streamlining of the SEDEX procedure. *Limnol. Oceanogr.* **45**, 509–515 (2000).
112. Jaisi, D. P. & Blake, R. E. Tracing sources and cycling of phosphorus in Peru Margin sediments using oxygen isotopes in authigenic and detrital phosphates. *Geochim. Cosmochim. Acta.* **74**, 3199–3212 (2010).
113. Ke, T. T., Zhang, D., Guo, H. M., Xiu, W. & Zhao, Y. Geogenic arsenic and arsenotrophic microbiome in groundwater from the Hetao Basin. *Sci. Total Environ.* **852**, 158549 (2022).
114. Wang, A. Characterization and biogeochemical significance of methanogens and methanotrophs in arsenic-rich groundwater. *Master thesis (in chinese)*, (China University of Geosciences, Beijing, 2021).
115. Bolyen, E. et al. Reproducible, interactive, scalable and extensible microbiome data science using QIIME 2. *Nat. Biotechnol.* **37**, 852–857 (2019).
116. Callahan, B. J. et al. DADA2: high resolution sample inference from Illumina amplicon data. *Nat. Methods* **13**, 581–583 (2016).
117. Li, Y. Phosphate-oxygen isotopes in groundwater of the Hetao Basin, China. Mendeley Data, V1, <https://doi.org/10.17632/2crfxdfwb.1> (2024).

Acknowledgements

This study was financially supported by the National Natural Science Foundation of China (grant No. 42130509 and 42307080), Project 111 (No. B20010), the Fundamental Research Funds for the Central Universities (grant Nos. 2652017165 and 2652017051), and the China Scholarship Council (CSC-University of Tübingen visiting PhD scholarship programme, file No. 201906400026). Many thanks to Flaiz, S., Fiedler, D., Hausner, L., and Rieber, C., who provide support to $\delta^{18}\text{O}_{\text{PO}_4}$ analyses in the laboratory of Soil Science and Geocology at the University of Tübingen. Special thanks to the valuable comments from editor and reviewers, which have greatly helped for improving the manuscript. The authors declare no permissions were required for the sediment sampling in this study.

Author contributions

Yao Li: Conceptualization, Visualization, Methodology, Writing – original draft, Writing – revision. Harald Neidhardt: Conceptualization, Methodology, Writing – review and editing, Supervision. Huaming Guo: Methodology, Resources, Writing – review and editing, Project administration, Funding acquisition, Supervision. Christiane Nagel: Laboratory analysis. Wen Shao: Laboratory analysis. Chen Yu: Investigation, Laboratory analysis. Bo Zhao: Investigation, Laboratory analysis. Dou Chen: Investigation, Laboratory

analysis. Wei Xiu: Conceptualization, Methodology. Yvonne Oelmann: Methodology, Resources, Writing – review and editing, Project administration, Funding acquisition, Supervision.

Competing interests

The authors declare no competing interests.

Additional information

Supplementary information The online version contains supplementary material available at <https://doi.org/10.1038/s43247-024-01666-3>.

Correspondence and requests for materials should be addressed to Huaming Guo or Yvonne Oelmann.

Peer review information *Communications Earth & Environment* thanks Federica Tamburini and the other, anonymous, reviewer(s) for their contribution to the peer review of this work. Primary Handling Editors: Annie Bourbonnais, Somaparna Ghosh, Martina Grecequet and, Alienor Lavergne. A peer review file is available

Reprints and permissions information is available at <http://www.nature.com/reprints>

Publisher's note Springer Nature remains neutral with regard to jurisdictional claims in published maps and institutional affiliations.

Open Access This article is licensed under a Creative Commons Attribution-NonCommercial-NoDerivatives 4.0 International License, which permits any non-commercial use, sharing, distribution and reproduction in any medium or format, as long as you give appropriate credit to the original author(s) and the source, provide a link to the Creative Commons licence, and indicate if you modified the licensed material. You do not have permission under this licence to share adapted material derived from this article or parts of it. The images or other third party material in this article are included in the article's Creative Commons licence, unless indicated otherwise in a credit line to the material. If material is not included in the article's Creative Commons licence and your intended use is not permitted by statutory regulation or exceeds the permitted use, you will need to obtain permission directly from the copyright holder. To view a copy of this licence, visit <http://creativecommons.org/licenses/by-nc-nd/4.0/>.

© The Author(s) 2024